ELUCIDATING THE FUNCTION AND EXPRESSION PATTERN OF A NOVEL ADENINE NUCLEOTIDE TRANSLOCASE, ANT4

By

JEFFREY VINCENT BROWER

A DISSERTATION PRESENTED TO THE GRADUATE SCHOOL
OF THE UNIVERSITY OF FLORIDA IN PARTIAL FULFILLMENT
OF THE REQUIREMENTS FOR THE DEGREE OF
DOCTOR OF PHILOSOPHY

UNIVERSITY OF FLORIDA

2008

To my loving parents, family and friends for all of their continued support and encouragement

ACKNOWLEDGMENTS

I would like to first thank my mentor, Dr. Naohiro Terada without whom none of this work would have been possible. Dr. Terada's constant wisdom, guidance, insight and friendship have been the reason for any success I have had during my graduate career. The environment that Dr. Terada creates for all of his graduate students is one of comfort and understanding while at the same time stimulation of critical thinking and innovation. I could never begin to express in words my absolute gratitude and respect for him. I would next like to thank Dr. Paul Oh who has been my "second" mentor. Dr. Oh's contributions to my development as a graduate student and individual have been immense and I can not begin to thank him enough. I would also like to thank all of my committee members, Dr. David Julian, Dr. Jim Resnick and Dr. Stephen Sugrue for their continued insight and essential assistance with my research. I would also like to thank our collaborator Dr. John McCarrey at the University of Texas at San Antonio for his significant contributions to my work.

Next, I would like to thank all of the members of the Terada lab, past and present, whom all have made a significant impact on my graduate career and overall happiness. In particular, Dr. Masahiro (Max) Oka, who oversaw a large part of my technical development, and also Dr. Takashi (Charlie) Hamazaki, Dr. Nemanja Rodic, Dr. Michael Rutenberg, Dr. Amar Singh, Dr. Sarah Kehoe, Dr. Brad Willenberg, Amy Meacham, and Katherine Hankowski.

I would like to give a special thanks to my parents, Clay and Cynthia, and my brother Jamie, whose love, support and encouragement are unwavering. Finally I would like to thank the rest of my family and friends who have supported me in many ways, without which I may have not been so successful in my graduate studies.

TABLE OF CONTENTS

page

LIST OF FIGURES

Abstract of Dissertation Presented to the Graduate School
of the University of Florida in Partial Fulfillment of the
Requirements for the Degree of Doctor of Philosophy

ELUCIDATING THE FUNCTION AND EXPRESSION PATTERN OF A NOVEL ADENINE NUCLEOTIDE TRANSLOCASE, ANT4

By

Jeffrey V. Brower

August 2008

Chair: Naohiro Terada
Major: Medical Sciences-Molecular Cell Biology

The adenine nucleotide translocases (Ant) facilitate the transport of ADP and ATP by an antiport mechanism across the inner mitochondrial membrane, thus playing an essential role in cellular energy metabolism. We recently identified a novel member of the *Ant* family in mouse, *Ant4*, of which gene configuration as well as amino acid homology is well conserved among mammals. The conservation of *Ant4* in mammals, along with the absence of *Ant4* in non-mammalian species, suggests a unique and indispensable role for this ADP/ATP carrier gene in mammalian development. Of interest, in contrast to its paralog *Ant2*, which is encoded by the X chromosome and ubiquitously expressed in somatic cells, *Ant4* is encoded by an autosome and selectively expressed in testicular germ cells. Immunohistochemical examination as well as RNA expression analysis using separated spermatogenic cell types revealed that Ant4 expression was particularly high at the spermatocyte stage. When we generated *Ant4* deficient mice by targeted disruption, a significant reduction in testicular size was observed without any other distinguishable abnormalities in mice. Histological examination as well as stage-specific gene expression analysis in adult and neonatal testes revealed a severe reduction of spermatocytes accompanied by increased apoptosis. Subsequently, the *Ant4* deficient male mice were infertile.

Taken together, these data elucidated the indispensable role of *Ant4* in murine spermatogenesis. Considering the unique conservation and chromosomal location of the *Ant* family genes in mammals, *Ant4* gene may have arose in mammalian ancestors and been conserved in mammals to serve as the sole and essential mitochondrial ADP/ATP carrier during spermatogenesis where the sex chromosome-linked *Ant2* gene is inactivated.

CHAPTER 1
INTRODUCTION

Mitochondria

The mitochondria are membrane enclosed organelles ranging in size from 1-10 μm and are found in most eukaryotic cells (1,2). The mitochondria are often described as the "power houses" of the cell due to the role they play in ATP production from ADP and P_i. They are responsible for the vast majority of the ATP produced for utilization by the cell in its many energy demanding processes. The mitochondria have also been implicated to play a role in ageing, the cellular death cascade, cell signaling, cellular differentiation, as well as growth and cell cycle control (3). Mitochondria have also been shown to play a role in many disease pathologies (mitochondrial mutations disease). The mitochondrion is believed to have arisen through the engulfment, by an early eukaryote, of a simpler bacterial prokaryote. These two organisms then developed a relationship in which both benefited and thus became symbionts.

Mitochondrial Structure

The mitochondria have a specialized structure in order to most efficiently support their numerous functions. The mitochondrion consists of both an inner and an outer membrane composed of phospholipid bilayers containing numerous proteins (2,4). The inner and outer membranes are separated by what is known as the intermembrane space. The invaginations of the inner membrane are known as cristae, and the region within the inner membrane is the matrix.

The mitochondrial outer membrane is composed of both a phospholipid bilayer and proteins, enclosing the organelle. The outer membrane has a phospholipid to protein ration of about 1:1 by weight, similar to the eukaryotic cell membrane (2,4). Contained within the outer membrane are integral proteins called porins which allow for the free diffusion of molecules of a

molecular weight of 5000 Daltons or less (2,4). There is a multi-subunit protein termed the translocase of the outer membrane that is able to actively move larger proteins containing an N-terminal signaling sequence, across the membrane and into the intermembrane space (5).

The intermembrane space contains a similar concentration of ions and sugars to that of the cytosol since the outer membrane is permeable to small molecules (4). The composition of larger protein molecules however, is quite different since they must possess a specific targeting sequence to be translocated into the intermembrane space (2,5).

The mitochondrial inner membrane contains the majority of the proteins that play a role in energy metabolism. The inner membrane contains proteins with essentially four types of functions, protein import, regulation of metabolite passage into and out of the matrix, the carrying out of the redox reactions essential to oxidative phosphorylation, and ATP synthesis (2,4). The protein to phospholipid ratio of the inner membrane is different from that of the outer membrane as the protein composition is much greater (3:1 by weight) (4). The inner membrane is also unique in that it is rich in an unusual phospholipid, cardiolipin, which was originally discovered in bovine hearts (6). Cardiolipin is unique in that it contains four fatty acids rather than the characteristic two, which may play a role in making the inner membrane more highly impermeable to all molecules (2,4). It is important to note that the mitochondrial inner membrane does not contain porins and almost all ions require a specific transporter to enter or exit the matrix compartment. This impermeability of the inner membrane is essential for the production of the membrane potential established by the action of the enzymes of the electron transport chain. The inner membrane contains folds known as cristae.

The cristae, which are formed by the invaginations of the inner membrane, are responsible for expanding the surface area of the inner membrane. This increased surface area provides more

space for the enzymes of the electron transport chain thus increasing the mitochondrion's ability to produce ATP. Cells which possess a higher demand for ATP, typically contain more cristae (4).

The space enclosed by the inner membrane is known as the matrix and contains approximately 2/3 of the total proteins present within the mitochondria (4). The matrix contains a mixture of enzymes, specialized mitochondrial ribosomes, tRNA, and mitochondrial DNA. A published human mitochondrial DNA sequence consisted of 16, 569 base pairs which encoded 37 total genes, 24 tRNA and rRNAs and 13 peptides (2,7). The mitochondrion has a specialized structure in order to carry out its many essential functions.

Mitochondrial Function

The mitochondria are most well known for the production of ATP for utilization during the cell's many metabolic processes (1,2,8). The mitochondrion however, is also involved in many other cellular pathways and processes.

The mitochondria are highly invested in the process of energy metabolism and rely on glycolysis, which occurs in the cytoplasm, to metabolize glucose. Briefly, glucose is phosphorylated by hexokinase to form glucose-6-phosphate which is subsequently rearranged to form fructose-6-phosphate. Fructose-6-phosphate is split by aldolase into two triose sugars, dihydroxyacetone phosphate and glyceraldehyde 3-phosphate (2,8-12). Dihydroxyacetone phosphate is rapidly converted into glyceraldehyde 3-phosphate by triosephosphate isomerase. The two molecules of glyceraldehyde 3-phosphate are then dehydrogenated and phosphorylated to make 1,3-biphosphoglycerate. The 1,3-biphosphoglycerate molecules are then converted into 3-phosphoglycerate and subsequently 2-phosphoglycerate. 2-phosphoglyecerate next becomes phosphoenolpyruvate which is finally converted into pyruvate. The pyruvate is then converted

into Acetyl CoA by pyruvate dehydrogenase which can subsequently enter the tricarboxylic acid cycle (TCA cycle). (2, 8-12) The process of glycolysis produces an overall 2 net ATP molecules.

The tricarboxylic acid cycle utilizes Acetyl CoA as the initial substrate. The TCA cycle takes place in the matrix of the mitochondria. Briefly, Acetyl CoA is converted into Citrate by Citrate synthase, which is next converted into Isocitrate by Aconitase. Isocitrate is then converted into α-ketogluterate by isocitrate dehydrogenase, which is subsequently converted into Succinyl-CoA by α-ketogluterate dehydrogenase. Succinyl-CoA is converted into Succinate by the Succinyl-CoA synthetase (2, 8-12). Succinate dehydrogenase then converts Succinate into Fumerate which is subsequently converted into Malate through the action of Fumarase. Malate is finally converted into Oxaloacetate by Malate dehydrogenase. The TCA cycle produces two net GDP molecules from each molecule of glucose. During this cycle NAD+ is reduced to NADH during the conversions of Isocitrate to α-ketogluterate, α-ketogluterate to Succinyl-CoA, and Malate to Oxaloacetate (2, 8-12). These reduced electron carriers are then utilized by the electron transport chain.

The electron transport chain is located along the mitochondrial inner membrane and is composed of a number of complexes (Complexes I-IV) that mediate the transfer of electrons along the transport chain. Complex I, also known as NADH dehydrogenase, accepts two electrons from NADH and transfers them to ubiquinone, a lipid soluble carrier which is able to diffuse readily through the membrane (2, 8-12). Complex I is also responsible for pumping two protons into the intermembrane space. Complex III, cytochrome bc1, accepts two electrons from the reduced ubiquinone (QH2) and transfers them to two molecules of cytochrome C one at a time. Complex III also pumps two protons into the intermembrane space (2, 8-12). Complex IV, also known as cytochrome c oxidase, next removes four electrons from four cytochrome c

molecules. Complex IV also pumps four protons into the intermembrane space. In turn complex IV transfers these electrons to the terminal electron acceptor, molecular oxygen producing water, thus the absolute necessity of O2. Next the F1FO ATP synthase utilizes the proton gradient that has been established by the coupled electron transport and hydrogen shuttling, to produce ATP from ADP and Pi (2, 8-12). The F1FO ATP synthase relies on the availability of ADP and also the removal of ATP for subsequent ATP production. This essential function is carried out by the adenine nucleotide translocases.

Adenine Nucleotide Translocases

The adenine nucleotide translocase/translocator (Ant), also called ADP/ATP carrier (Aac), belongs to the mitochondrial solute carrier family which supports a variety of transport activities across the mitochondrial inner membrane (13-19). The Ant proteins facilitate the exchange of ADP/ATP by an antiport mechanism across the inner membrane of the mitochondria, (13,15,16) and thus are considered to be essential for the utilization of ATP produced by oxidative respiration (13-16,20). The Ant proteins are also thought to be an integral component of the mitochondrial permeability transition pore (21-23), although this function is still in question (24).

The Ant proteins are the most abundant proteins of the mitochondrial inner membrane and are comprised of approximately 300-320 amino acid residues which form six transmembrane helices. The functional unit is likely a homodimer acting as a gated pore that channels single molecules of ADP and ATP (25) Until recently, it has been believed that humans posses three members of the *ANT* family of genes: *ANT1* (*SLC25A4*), which is expressed primarily in the heart and skeletal muscle; *ANT2* (*SLC25A5*), which is expressed in rapidly growing cells and is inducible; and *ANT3* (*SLC25A6*), which appears to be constitutively expressed in all tissues (26,27). In contrast, rodents were believed to possess only two members of the *Ant* family: *Ant1* which is expressed at high levels in heart, skeletal muscle, and brain; and *Ant2* which is

expressed in all tissues but skeletal muscle (14). Mouse *Ant2* is the ortholog of human *ANT2* and seems to combine the functions of human *ANT2* and *ANT3* (28,29). Genetic inactivation of *Ant1* resulted in viable mice (15). However, these animals developed mitochondrial myopathy and severe exercise intolerance along with hypertrophic cardiomyopathy (15,19). In humans, there is a clinical manifestation known as autosomal dominant progressive external opthalmoplegia (adPEO) which is associated with *ANT1* as well as *TWINKLE*, and *POLγ* mutation (30). This disorder is characterized molecularly by the accumulation of numerous mitochondrial DNA mutations and clinically by the appearance of external opthalmoplegia, ptosis, and progressive skeletal muscle weakness (31). In the cases of *ANT1* mutation, A114P, L98P, A90D, D104G, and V289M substitutions have been reported to be associated with adPEO (32). Gene disruption of *Ant2* in mice appears to result in embryonic to perinatal lethality, although a detailed phenotype has not yet been published (http://www.patentdebate.com/PATAPP/20050091704). There have been no reports regarding *ANT2* or *ANT3* mutations in human.

Adenine Nucleotide Translocase 4

Utilizing various approaches, we and others recently identified a novel member of the *Ant* family, *Ant4*, both in mouse and human (16,17,33). The mouse *Ant4* gene was predicted to encode a 320 amino acid protein, and shared amino acid sequence homology with the other mouse Ant proteins previously identified (70.1% and 69.1% overall amino acid identity to Ant1 and Ant2, respectively). The *Ant4* gene also contained three tandem repeats of a domain of approximately 100 residues, each domain containing two transmembrane regions, a characteristic shared by all members of the Ant family (34). Dolce et al. demonstrated that human ANT4 (AAC4) indeed localizes to mitochondria in cells and can actively exchange ADP for ATP by an

electrogenic antiport mechanism *in vitro*. Of interest, the *Ant4* gene is expressed selectively in the testis, both in mouse and human (17,33).

Spermatogenesis

The recently discovered Ant4 is expressed exclusively within the testis. The testis are composed of both somatic and germ cell populations. Within the testis is an extensive network of tubular structures known as the seminiferous tubules (35, 36). The seminiferous tubules are the sight of a highly specialized process known as spermatogenesis. Spermatogenesis is the process by which a resident stem cell population gives rise to differentiating and maturing cells which eventually become mature sperm.

Spermatogenesis occurs within the seminiferous tubules of the testis and commences within the stem cells of the testis the spermatogonial cells (type A), located along the basal lamina (37). The type A spermatogonia undergo an asymmetric mitotic cell division to give rise to another type A and a type B spermatogonium. The type A spermatogonial cells proliferate repeatedly and are responsible for the constant replenishment of the germinal cell population within the seminiferous epithelium (36). The type B spermatogonia, which are the last cell type of the seminiferous epithelium to be produced by means of a mitotic division, are committed to enter meiosis I as primary spermatocytes. The process of meiosis is unique to gametogenesis and is essential for the production of haploid gametes and thus preservation of the species.

Meiosis I

Meiosis is a highly specialized process restricted to the germinal cells of the gametes. Meiosis I is initiated in the primary spermatocytes and is separated into interphase, prophase, metaphase, telophase, and anaphase (38-41). During interphase the chromosomes replicate, prior to prophase I. By prophase I of meiosis I, which is an elongated prophase in comparison to prophase of mitosis and meiosis II, the chromosomes have replicated. This elongated prophase is

further broken down into leptotene, zygotene, pachytene, diplotene and diakinesis (40,41). During leptotene the individual chromosomes begin to condense, forming long strands present within the nucleus. At this point, sister chromatids are tightly associated with one another as to be indistinguishable. Following leptotene is zygotene, during which time the chromosomes condense further and become visibly distinguishable as long thread-like starnds. At this point, homologous chromosomes begin to seek out one another and initiate the process of synapsis. This synapsis is mediated through the synaptonemal protein complex which allows homologous chromosomes to align along their lengths and form tight associations with one another. The next stage of prophase I is pachytene. During pachytene the complete condensation and synapsis of homologous chromosomes is completed. The now completely synapsed homlogous chromosomes are referred to as bivalents or tetrads due to the presence of the two sister chromatids of each homologue (40). Pachytene is a very important stage of meiosis, as it is responsible for the generation of genetic diversity. This genetic diversity arises from the random process of genetic exchange that occurs between nonsister chromatids of homologous chromosomes. Following pachytene is the stage known as diplotene. During diplotene the synaptonemal complex begins to degrade and homologous chromosomes begin to separate from one another, remaining tightly associated at chiasmata, the regions where crossing-over occurred. During the next stage, diakinesis, the chromosomes further condense and the nuclear membrane disintegrates and the meiotic spindle begins to form (40,41). Following prophase I is metaphase I, during which kinetochore microtubules from both centrioles attach to the kinetochores of homologues. The homologous chromosomes align along the equatorial plate due to a continuous force exerted in a counterbalancing manner by the microtubules upon the bivalents. Random assortment is generated based upon the random orientation of the bivalents about the metaphase

plane (38,40). Next the microtubules attached at the kinetochores shorten and pull homologous chromosomes apart, towards opposing poles, during anaphase I (40). Following anaphase I the centromeres arrive at the poles and each daughter cell now possesses half the number of chromosomes. However, each chromosome consists of two sister chromatids. Cytokinesis occurs, which is the pinching of the cellular membrane as to form two cells (38). The cells now enter a resting state known as interphase II. During the above described process of meiosis I, the diploid primary spermatocytes have undergone a reductive division, effectively halving their chromosomal content. Subsequently meiosis II ensues, during which the secondary spermatocytes undergo an equational division. At this point the primary spermatocyes become secondary spermatocytes as they enter meiosis II.

Meiosis II

The secondary spermatocytes proceed through the stages of meiosis II, consisiting of interphase, prophase, metaphase, anaphase and telophase (38-41). These stages are similar to meiosis I except that prophase I is not broken down into sub-stages as it was in meiosis I. Briefly, during prophase II the nuclear envelope disappears, and the chromatids condense, in metaphase II the microtubules associated with the kinetochore and attach at the polar centrioles resulting in the formation of a metaphase II plate, oriented perpendicular to the metaphase I plate (40). Next during anaphase II the sister chromatids are separated and moved to opposing poles. Following anaphase II is telophase II which is similar to telophase I during which chromosomes uncoil and lengthen, nuclear envelopes form and cellular cleavage occurs (38). The result is four haploid cells which exit meiosis and become sparmatids.

Spermiogenesis

Spermatids are the haploid results of meiosis. Spermatids undergo further maturation and terminal differentiation during the process known as spermiogenesis. There are three major

changes through which the spermatids must undertake. First the nucleus elongates and histones are replaced with protamines which allow for the establishment of highly condensed chromatin. This highly condensed transformation of the chromatin is necessary in order to accommodate the significantly reduced cytosolic and nuclear compartments of the sperm. Next the Golgi apparatus produces a lysosomal-like granule that forms above the nucleus, towards the tip of the developing spermatid. This lysosomal granule will form the future acrosome which is an essential component of the penetration of the zona pellucida and subsequent sperm/egg fusion (36). Finally the spermatid elongates and forms a tail along which mitochondria are deposited in the proximal region. Also excess cytoplasm is released as the residual cytoplasmic body (36). Following the morphological changes that occur to the spermatids as they mature, release of spermatozoa into the seminiferous tubule lumen occurs by the process of spermiation (36). The entire process of spermatogenesis relies heavily on the somatic constituent of the testicular environment.

Somatic Cell Supportive Function

The somatic cells present within the seminiferous epithelium provide support and direction to the developing germ cells in various ways, and thus play an important role in the development of the germ cell compartment of the testis. The Sertoli cell extends from the basement membrane to the lumen of the seminiferous epithelium and is responsible for supporting and protecting the developing germinal cells (36). The Sertoli cells have both endocrine and structural roles in the development of the germ cells as they secrete a number of substances which have profound effects on the maturation and progression of the germ cells.

Sertoli cells are responsible for the production and secretion of a number of factors necessary for the maintenance and maturation of the germ cells (42,43). Some such factors secreted by the Sertoli cells are, inhibins and activins, which together work to regulate the

secretion of FSH from the pituitary gland, glial cell-line derived neurotrophic factor (GDNF), which plays a role in undifferentiating spermatogonial cell progression, and the Ets related molecule (ERM), which is needed for spermatogonial stem cell maintenance, to name a few (42,43). The Sertoli cells also play a very important role in the structural support of the developing germ cell compartment.

The Sertoli cells are often referred to as the "nurse" or "mother" cells of the seminiferous epithelium (36). In addition to providing secretory support, they also are responsible for the structural and directional support of the germ cells. Sertoli cells are in direct contact with the maturing germ cells from the spermatogonial stage all the way until their release into the seminiferous epithelium as late spermatids. The tight junctions present between adjacent Sertoli cells are responsible for the establishment and integrity of the blood-testis barrier (36, 42). This Sertoli cell interaction separates the seminiferous epithelium into basal and adluminal compartments. This blood-testis barrier mediated by Sertoli cell tight junctions, is responsible for determining which molecules enter and exit the adluminal compartment. The blood-testis barrier also makes the adluminal compartment and immune privileged site (42). The Sertoli cells also determine when the maturing and differentiating spermatogonial cells will pass through the tight junctions and into the adluminal compartment. Without the function of intact Sertoli cells, spermatogenesis can not occur (42).

CHAPTER 2
MATERIALS AND METHODS

Immunostaining

Testes were harvested from 6-week-old wild-type or mutant male mice. All mice have been maintained under standard specific-pathogen-free (SPF) conditions, and the procedures performed on the mice were reviewed and approved by the University of Florida Institutional Animal Care and Use Committee (IACUC). The tissues were then fixed in a mild fixative (10% formalin) overnight with rocking. Following fixation the tissues were dehydrated using an organic solvent (beginning with PBS and working towards more dehydrating solutions such as Citrasol). The tissues were then imbedded in paraffin and sectioned. Formalin-fixed, paraffin embedded human testis tissue was obtained through the University of Florida Department of Pathology tissue bank. Use of human tissue was performed in accordance with IRB-approved protocols at the University of Florida. Tissues were re-hydrated with organic solvents of decreasing concentrations (beginning with Citrasol and moving towards more hydrating solutions and ending with PBS). Deparaffinized and re-hydrated 5 μm tissue sections were stained with rabbit polyclonal antibodies against mouse Ant4, or a cleaved Caspase-3 (Cell Signaling Technologies, Danvers, MA). Slides were blocked for endogenous peroxidase activity and then unmasked in Target Retrieval Solution (Dako, Carpinteria, CA). Antibody was applied at 1:600 (Ant4) or 1:200 (Caspase-3) for one hour at room temperature prior to identification using the DAB Envision kit (Dako). An isotype and concentration matched negative control section was included for each tissue. Slides were counterstained with hematoxylin. For immunostaining of human ANT4, rabbit polyclonal antibodies were raised against the N-terminal human ANT4 peptide (REPAKKKAEKRLFDC) and purified through an affinity column using the same peptide (Sigma Genosys, The Woodlans, TX).

Preparation of Stage-specific Spermatogenic Cells

Stage-specific spermatogenic cells were prepared from neonatal, prepubertal and adult CD-1 mice by sedimentation through a 2-4% BSA "Sta Put" gradient at unit gravity as described previously (44). Specifically, primitive type A spermatogonia were recovered from testis of male mice at 6 days postpartum (dpp). Similarly, type A and type B spermatogonia were recovered from males at 8dpp, preleptotene, leptotene + zygotene, and juvenile pachytene spermatocytes were recovered from males at 18 dpp, and adult pachytene spermatocytes, round spermatids and residual cytoplasmic bodies were recovered from males at 60+ dpp. Purities of recovered cell types were assessed on the basis of morphological characteristics when viewed under phase optics and were ≥85% for prospermatogonia, spermatogonia, and juvenile spermatocytes (preleptotene, leptotene plus zygotene, and juvenile pachytene) and ≥95% for adult pachytene spermatocytes and round spermatids (44).

Real-Time PCR

Total RNA was extracted using the RNA aqueous kit (Ambion). cDNA was synthesized using the HiCapacity cDNA Archive kit using random primers (Applied Biosystems, Foster City, CA). Briefly, 10 μL Reverse Transcription Buffer, 4 μL 25X dNTPs, 10 μL 10X Random Primers, 5 μL MultiScribe Reverse Transcriptase, and 21 μL of nuclease-free H_2O was incubated with 50 μL of RNA (2 μg). Reaction consisted of two steps, first a 25˚C incubation for 10 minutes, and second a 37˚C incubation for 120 minutes.

Real-time PCR reaction was performed using the TaqMan Gene Expression Assay (Applied Biosystems) according to manufacturer's instructions. Each 20 μL reaction consisted of 10 μL of TaqMan Universal PCR Master Mix, No AmpErase-UNG; 1 μL of TaqMan Gene Expression Assay Mix, for *β-actin* (VIC-labeled), *Ant4* (FAM-labeled), or *Ant2* (FAM-labeled); and 9 μL of cDNA (50 ng). Reactions were performed using Applied Biosystems 7900HT Fast

Real-Time PCR instrument. Gene expression analysis was performed using the comparative CT method using *β-actin* for normalization.

Targeting Vector Construction

The targeting vector was designed to replace exons 2-4 of the mouse *Ant4* gene with an SV40 splicing donor/acceptor signals-IRES (internal ribosomal entry site)-ßgal-and PGKneor (neomycin resistant gene cassette driven by the PGK promoter) cassette of the pNF-SIBN targeting vector. The targeting construct was generated by sequential subcloning of the 5' homology arm, 3' homology arm, and diphtheria toxin gene into the pNF-SIBN vector. A 2.0 kb fragment containing exon 1 and a 5.3 kb fragment containing exons 5-6 was amplified from mouse ES cell (R1, 129/SvJ strain) genomic DNA and used as the source of 5' and 3' homologous arms for the targeting constructs, respectively. Targeting arms were amplified by LA Taq PCR system (Takara, Madison, WI) with the following primers Ant4-5.f (5-CCGCTCGAGCTCTCATTGTTTTAACTGGATACGTG), Ant4-5.r (5-GCGTGTCGACTGGCCCTGCACATTCTCCAAAACACC), Ant4-3.f (5-CCCGCTCGAGGAGTAATTGGTGACTTTAAGTGG) and Ant4-3.r (5-GCGTGTCGACTGCTCACTAAATGGACTCTGGG). The homologous arms were cloned into pCR 2.1-TOPO vector (Invitrogen, Carlsbad, CA). Following excision from pCR2.1-TOPO vectors, the 5' homologous arm was ligated into the XhoI site, and the 3' homologous arm was ligated into the SalI site in the pNF-SIBN targeting vector. To increase selection efficiency of positive clones, we inserted the negative selection gene (diphtheria toxin) into the XhoI site.

Generation of Ant4$^{-/-}$ Mice

The targeting vector was linearized with SalI digestion, and transfected into J1 ES cells by electroporation as we previously described (45). Genomic DNA from ~450 G418-resistant colonies was screened, and homologous recombination in ES cells confirmed by genomic

Southern blotting. Upon initial Southern blot screening with a 5' external probe followed by confirmation with a 3' internal probe, three successfully targeted ES clones were identified. ES cells from one positive clone were injected into blastocysts of the C57BL/6 (B6) strain. Chimeric male mice were mated with females on a B6 background.

Southern Blotting

Genomic DNA was extracted using the DNA Wizard Genomic DNA purification Kit (Promega, Madison, WI, http://www.promega.com). Briefly, mouse tails clips were performed to obtain tissue. Tissue lysis solution was prepared by adding 120 µL of a 0.5M EDTA to 500 µL of Nuclei Lysis Solution and chilled on ice until solution turns cloudy. Next 600 µL of the lysis solution was added to 0.5-1 cm of fresh mouse tail in a 1.5 ml microcentrifuge tube. To the solution was added 17.5 µL of 20 mg/ml Proteinase K. Samples were then incubated overnight in a 55˚C water bath with gentle shaking. Following overnight incubation, 3 µL of RNase solution was added to the nuclear lysate, mixed by inversion and incubated at 37˚C for 17 minutes. The samples were then allowed to cool to room temperature for approximately 5 minutes. Next, 250 µL of Protein Precipitation Solution was added to the room temperature samples and placed at -20˚C for approximately 5 minutes. Following incubation at -20˚C the samples were centrifuged for 5 minutes at 15,700 g. The precipitated protein will form a tight white pellet. The supernatant was carefully removed and transferred to a clean 1.5 ml microcentrifuge tube containing 600 µL of room temperature isopropanol. The samples were then gently mixed by inversion until white thread-like strands of DNA began to be visible. The samples were then centrifuged for 5 minutes at 15,700 g. The DNA was visible as a small white pellet and the supernatant was carefully removed. Next, 600 µL of room temperature 70% ethanol was added and the tubes were vortexed gently and briefly to wash the pellet. The samples were then centrifuged for 1 minute at 15,700 g and the supernatant was removed carefully. The tubes were then inverted on a paper

towel and left to air-dry for 15 minutes. Following air-drying at room temperature, the samples were placed into a heat block set to 90˚C for 1-3 minutes to ensure proper drying. The samples were then rehydrated by placing them in 100 μL of DNA rehydration solution overnight at 4˚C. The genomic DNA was then deigested with BamHI and separated in 1% agarose gels. After denaturation and neutralization of the gel, DNA was transferred to nylon membranes and hybridized with specific 5' external and 3' internal probes.

PCR Genotyping

In order to rapidly and effectively determine the genotype of the resultant mice of set matings, we developed a PCR based genotyping technique. Genomic DNA was extracted using the DNA Wizard Genomic DNA purification Kit (Promega, Madison, WI, http://www.promega.com). The DNA samples then underwent a PCR amplification using primers specific for each allele. For the Ant4 targeted allele the forward primer was designed in intron 1, and the reverse primer was designed at the splicing donor/acceptor site of the β-gal-PGK-neomycin cassette. Primers F- GTTTTGGAGAATGTGCAGGG, R-GCAACATCCACTGAGGAGCAGTTC. The resulting amplicon was approximately 250 bps. In order to detect the wild-type allele, we designed primers to amplify the exon-intron 2 region which was absent from the targeted allele. The forward primer was designed in exon 2 and the reverse primer was designed in intron 2. Primers F- GGCAATTTGGCAAATGTTATTCG, R-GCGATCCCTAGTTACTGAAACTAAG. The resulting amplification product was approximately 350 bps. In order to effectively amplify from a genomic template, we designed a genomic specific PCR program. Genomic PCR: step 1- 90˚C for 15 minutes, step 2- 94˚C for 1 minute, step 3- 55˚C for 1 minute, step 4- 72˚C for 1 minute, step 5- go to step 2 and repeat 39 times, step 6- 72˚C for 10 minutes, hold at 4˚C.

Immunoblotting

We used testis and heart samples from 6 wk-old-mice for western blotting. For testis and heart, tissues were frozen using liquid nitrogen and mechanically minced with a razor blade.The cells were then lysed in RIPA buffer, and 35 μg of total protein was separated by sodium dodecyl sulfate-10% polyacrylamide gel elctrophoresis and transferred to a nitrocellulose membrane. The following were used as primary antibodies; the rabbit polyclonal antibodies against Ant4 as we previously described (17), Anti-Ant1 and Ant2 antibodies provided by Douglas C. Wallace (UC Irvine); Actin (sc-1615 Santa Cruz, Santa Cruz, CA); and GAPDH (RDI-TRK5G4-6C5 Research Diagnostics, Flanders, NJ). Peroxidase-conjugated immunoglobulin G (Santa Cruz) was used as the secondary antibody, followed by enhanced chemiluminescence (ECL) detection (Amersham, Piscataway, NJ).

RT-PCR Analysis

We isolated total RNA from testes of wild-type, heterozygous and homozygous mutant 6wk-old-mice using the RNA aqueous kit according to manufacturer's instructions (Ambion, Austin, TX). Briefly testes were removed dissected into two equal halves and tunica albugenia were removed. The seminiferous tubules were then finely minced with a razor blade. The minced tissue was then placed in 350 μL of Lysis/Binding solution and gently vortexed to lyse the tissue. An equal volume of 64% ethanol was added and the lysate was spun through a filter cartridge at 13,000 RPM for 1 minute in a tabletop centrifuge. The cartridge was washed with 700 μL Wash Solution 1, then two more times with 500 μL Wash Solution 2. RNA was eluted by adding 35 μL o pre-warmed Elution Solution.

The cDNA was synthesized using a SuperScript II first-strand synthesis system with oligo(dT) (GIBCO BRL, Grand Island, NY). PCR was performed using Taq DNA polymerase (Eppendorf, Westbury, NY). RT step was performed by mixing 1 μL Oligo(dt), 1 μL 10mM

dNTP, and 1-2 µg of total RNA, and DEPC-H_2O to a final volume of 10 µL. Mixture was incubated at 65˚C for 5 minutes, and then 4˚C for 2 minutes. Next, 9 µL of reaction m ixture consisting of 2 µL 10X PCR buffer, 2 µL 0.1 M DTT, 4 µL 25mM $MgCl_2$ and 1 µL of RNaseOUT, was added to the reaction and incubated at 42˚C for 2 minutes. Then, 1 µL of SuperScript RT was added to the mixture and the reaction was performed at 42˚C for 50 minutes. The reaction was terminated by a 15 minute incubation at 70˚C. The RNA was degraded by addition of 1 µL RNase H at 37˚C for 20 minutes. The cDNA was diluted up to 200 µL with water. The PCR reaction was performed by incubating 5 µL of cDNA with 0.25 µL of 50 µm each primer, 0.5 µL 10mM dNTPs, 2.5 µL 10X PCR buffer, 0.125 µL Taq in a final volume of 25 µL. The PCR reaction consisted of the following steps: a preliminary incubation of 94˚C for 3 minutes, then 94˚C for 1 minute, 55˚C for 1 minute, 72˚C for 1 minute, and repeated to step 2, 29 more times. For each gene, primers were designed from different exons, avoiding pseudogenes, and being sure that the PCR product would represent the RNA target and not background genomic DNA. Primer sequences: Ant4 F-GGAGCAACATCCTTGTGTG, Ant4 R-AGAAATGGGGTTTCCTTTGG, Dazl F-GCCAGCACTCAGTCTTCATC , Dazl R-GTTGGAGGCTGCATGTAAGT, Dmc1 F-GGCCTCCGCGTTCTGGGTCG, Dmc1 R-CTCATCATCTTGGAATCCCGATTCTTCC, A-Myb F- , A-Myb R- , Dvl3 F-CAGCATCACAGACTCCA, Dvl3 R-CAGCCTGCACCGGCAAATC, Sycp3 F-GCAGAGAGCTTGGTCGGGGCC, Sycp3 R-CTGAACCAGACAGATCTTTATCATCTTTC, Cyclin A1 F-GAGAAGAACCTGAGAAGCAGG, Cyclin A1 R-CTGGCCACAGGTCCTCCTGTAC, HoxA4 F-GAAGGGCAAGGAGCCGGTGGTG, HoxA4 R-CTCCGGTTCTGAAACCAGATCTTG, Dvl1 F-TGAGACAGGCACAGAGT, Dvl1 R-

GTCTGGGACACGATCTC, β-Actin F-ATGGATGACGATATCGCT, β-Actin R-ATGAGGTAGTCTGTCAGGT

TUNEL Assay

Paraformaldehyde fixed, paraffin embedded sections (5 μm) were de-paraffinized and re-hydrated through a graded series of ethanol through water. Slides were then placed in 0.1M citrate buffer pH 6.0 and permeabilized by exposure to 6 minutes of microwave irradiation (350W). Staining was performed using the In Situ Cell Death Detection Kit (Roche Applied Science, Indianapolis, IN) following the manufacturer's instructions. TUNEL reaction mixture containing TdT and fluorescein-dUTP was incubated on the slides for 1 hour at 37^{o}C, with negative control slides receiving labeling mixture devoid of TdT enzyme. After 3 washes in 1X PBS, slides were cover-slipped using Vectorshield with DAPI (Vectorlabs, Burlingame, CA). In some experiments, fluorescein-dUTP was visualized using anti- fluorescein antibody conjugated with alkaline phosphatase.

X-gal Staining

Testes were harvested from 6-week-old wild-type (+/+), heterozygous (+/-), and homozygous (-/-) mutant male mice and dissected into two equal halves. The tissues were then fixed in a mild fixative (10% formalin) for approximately 10-15 minutes. Following brief fixation, X-gal staining was carried out overnight with rocking, in order to prevent misshaping of the organ. The samples then underwent post fixation to further ensure the integrity of the tissue. Following post fixation the tissues were dehydrated using an organic solvent (PBS-Citrasol). The tissues were then imbedded in paraffin and sectioned. Following paraffin imbedding the tissues were re-hydrated with organic solvent (Citrasol-PBS) of decreasing concentrations. Slides were counterstained with hematoxylin.

Meiotic Chromosomal Spreads

Meiotic chromosomal spreads were prepared using a protocol similar to that in Peters et al. (1997). Briefly, testes were freshly dissected from adult mice (6 weeks) and decapsulated. Tunica albuginea was removed by physical dissociation following the dissection of the testis into two equal halves. Extratubular tissue was removed by rinsing the seminiferous tubules with PBS in the lid of a Petri dish. Following rinsing, the seminiferous tubules were blotted on a paper towel to remove any excess PBS. Tubules were then placed in approximately 1 ml of hypotonic extraction buffer (30mM Tris, 50mM sucrose, 17mM trisodium citrate dehydrate, 5mM EDTA, .5mM PMSF, pH 8.2) inverted 3-6 times and incubated at room temperature for 30-50 min. Following incubation, one-inch lengths of tubules were dissected out and placed in 20µL of sucrose solution (100mM sucrose pH 8.2, set with NaOH) and torn, into small pieces with fine forceps. The volume was then increased to 40µL with sucrose solution and pipetted to give a cloudy suspension, which was spread onto two slides dipped in formaldehyde solution (1% formaldehyde, 0.15% Triton-X100 in water adjusted with sodium borate to pH 9.2). Note: it is very important that the formaldehyde solution be made up fresh every time, as the pH may fluctuate and affect the fixation and spreading process. Slides were then air-dried for 2-3 hrs in a humidified chamber and then left to air-dry for the remainder of the time until the slides were dry,and used immediately or stored at -20/-80°C. For immunostaining, slides were rinsed for 5 min in PBS and then incubated for 30 min in wash/dilution buffer (3% BSA, .5% Triton X100 in PBS). This protocol was adapted from Nickerson et al. 2007. Spermatocytic preparations were incubated with both rabbit polyclonal Sycp3 (Ab15092, Abcam) and mouse monoclonal γH2AX (Ab22551, Abcam) at 1:200 dilutions. Antibodies were diluted in wash/dilution buffer and incubated at 4°C overnight. Following three 3-min washes in PBS, fluorescent conjugated

secondary antibody, diluted 1:2000 in wash/dilution buffer, were added and incubated for 45 min at room temperature in the dark. Sycp3 staining was visualized with an Alexa-fluor 488-conjugated anti-rabbit secondary antibody and γH2AX was visualized with a Cy3-conjugated anti-mouse secondary antibody. Slides were then washed in PBS, stained and mounted with Vectashield (Vector Laboratories, Inc. Burlingame, CA 94010) containing DAPI. DAPI was added to slides to visualize DNA.

Promoter Analysis

The promoter regions of *Ant1*, *Ant2*, and *Ant4* were analyzed for the presence of CpG islands using the MethPrimer program (http://www.urogene.org/methprimer/index1.html). Briefly, sequences containing 500 bp upstream of the transcription start site and 212 bp downstream, were entered and searched by MethPrimer for CpG islands, for *Ant1*, *Ant2*, and *Ant4*. The predictions were then further confirmed by sequence analysis of these regions.

Bisulfite Sequencing and Combined Bisulfite Restriction Analysis

DNA was extracted from various tissues using the DNA Wizard Genomic DNA purification Kit (Promega, Madison, WI, http://www.promega.com). Testes were decapsulated, and seminiferous tubules were collected for analysis. A bisulfite reaction was performed using the EZ DNA Methylation Kit (Zymo Research, Orange, CA, http://www.zymoresearch.com). Briefly Up to 2 μg of genomic DNA was used for conversion with the bisulfite reagent. Approximately 80 ng of bisulfite-converted DNA was used as template for each PCR analysis. The polymerase chain reaction (PCR) was performed in 25 μL reaction mixtures containing 2 μL of bisulfite converted DNA (50-100ng), 1 μM of primers, .625 U of HotStar Taq (Qiagen, Maryland, USA), 200 μM deoxy-nucleotide triphosphates and .25x Qsolution. Primers used for combined bisulfite restriction analysis (COBRA) were *Ant1*: 5'-GGAAGGGGTGGAAGTTTG and 5'-CTAATCCCCCATACTAAAAACC; *Ant2*: 5'-GGTTTGATTAGGTGTTAAGGGTAAG

and 5'-ACATCTATCATATTAAAAACAAAAA; *Ant4*: 5'-GTAGTATTTGGTTAGAGTGTGTTTTTTGG and 5'-ACACTAAAAAAAACTAAAAAACC (40 cycles). Following PCR amplification, fragments were purified using a PCR purification kit (Qiagen) and eluted into a final volume of 35 µL. Digestion of PCR purified fragments was then carried out with HhaI as follows: 35 µL eluted PCR purified fragments, 4.5 µL of NEB buffer 4 (New England Biolabs, Beverly, MA), 1.5 µL of HhaI enzyme (New England Biolabs), .25 µl of Bovine serum albumin (New England Biolabs), and 3.75 µL water. Digestion was carried out overnight and products were subsequently subjected to electrophoresis at 100V for 30min. on 2% agarose gels. Primers used for bisulfite sequencing were *Ant1*: 5'-TGTTTAGGGATTAGTTTAGTTAATG and 5'- CTAATCCCCCATACTAAAAACC; *Ant2*: 5'-GGTTTGATTAGGTGTTAAGGGTAAG and 5'- ACATCTATCATATTAAAAACAAAAA; *Ant4*: 5'-TTGTTGTGTATTGATTGAGTATG and 5'- ACACTAAAAAAAACTAAAAAACC. PCR fragments were cloned into pCRII-TOPO cloning vector (Invitrogen, Carlsbad, CA, http://www.invitrogen.com), and individual clones were sequenced.

CHAPTER 3
RESULTS

Ant4 Phylogeny

As one of many steps in determining the function of Ant4 we decided to investigate the similarities and differences between Ant4 and the other Ants. In order to do this, we carried out a phylogenic analysis of the adenine nucleotide translocases, which was based on the amino acid sequences of each Ant.

The Autosomal Ant4 Gene is Conserved in Mammals

The deduced amino acid sequence of *Ant4* is well conserved among mammals (around or over 90%) (Table 2-1); however, a phylogram indicates that *Ant4* is relatively distinct from the other mammalian Ant family peptides, Ant1, 2 & 3 (Fig. 3-1). Indeed, the amino acid identity between Ant4 and other Ants is approximately 70%. Of interest, the gene configuration of *Ant4* is also well conserved among mammals, but different from that of other *Ant* members. The *Ant4* gene always consists of 6 exons whereas the other *Ants* have 4 exons in all mammalian species investigated. Another distinguishing characteristic of mammalian *Ants* is in their chromosomal location. The *Ant1* gene, which is predominantly expressed in skeletal muscle and heart, is on an autosome. The *Ant2* gene, which is ubiquitously expressed in somatic organs, is encoded by the X chromosome and the *Ant3* gene which has been identified in only a portion of mammalian species so far, including human, cow and dog is also located on the X chromosome. Rodents apparently do not possess the *Ant3* ortholog, based on a search of the published genome databases. *Ant3* has the highest homology with *Ant2*, and is ubiquitously expressed in somatic organs like *Ant2*. It should be noted that the human *ANT3* gene is localized to the tip of the short arm (Xp22) of the X chromosome, which is known as the pseudoautosomal region 1 (PAR1). In contrast to *Ant2* and *Ant3*, the *Ant4* gene is always encoded by an autosome. Moreover, in

contrast to *Ant1* and *Ant2*, of which orthologs are found in other species including amphibians and fish, the *Ant4* gene apparently exists only in mammals including the marsupials. *Ant4* is found in both eutherian and metatherian species suggesting the presence of *Ant4* in their common therian ancestor. The eutherian radiation event representing the divergence of eutherian and metatherian lineages occurred ~150 million years ago suggesting that the emergence of *Ant4* occurred at least 150 million years ago (44,46), relatively close to the origin of mammals (~200 million years ago).

Ant4 Expression Pattern

The exact expression profile of Ant4 in testis had not been determined. In order to gain insight into the possible function of Ant4 within the testis we sought to determine the exact expression pattern of Ant4, and thus determine which cell types relied on Ant4. We demonstrated in a previous publication that Ant4 protein was expressed in testicular germ cells of mice (17); however, due to the limited resolution we obtained during immunostaining of cryopreserved tissues, we were unable to further define the exact expression profile of the protein within the testis at that time. As a result, we chose to utilize an alternative tissue preparation technique in order to increase the sensitivity of our analysis.

Ant4 Expression is Highest in Primary Spermatocytes

Utilizing paraffin-embedded formalin-fixed tissues we were able to determine more precisely the expression pattern of Ant4 in mouse testis. Of interest, it appears that Ant4 protein expression is highest in spermatocytes among testicular germ cells, based upon nuclear morphology and position within the seminiferous epithelium (Figure 3-2). Interestingly, mouse sperm also possess Ant4 protein within the midpiece or neck region (Figure 3-3). We also examined the expression pattern of ANT4 in human testis samples using polyclonal antibodies raised against human ANT4 and were able to more clearly distinguish the cell types within

which ANT4 was expressed (Figure 3-4). The human immunohistochemistry data provided us with evidence that primary spermatocytes express the highest levels of the ANT4 protein, whereas spermatogonial cells express a lower level. Importantly, Sertoli cells or other somatic interstitial cells did not express ANT4. In order to further define the stage specific-expression of Ant4 in male germ cells, we analyzed *Ant4* mRNA expression in separated spermatogenic cell types of mouse using real-time RT-PCR analysis (Figure 3-5). *Ant4* transcript levels began to increase upon transition of premeiotic type B spermatogonia into the early stages of meiosis as represented by preleptotene spermatocytes (PL). The transcript level of *Ant4* continued to increase through the leptotene and zygotene spermatocyte stages, peaking in early pachytene spermatocytes. *Ant4* transcript levels then began to decrease in late pachytene spermatocytes and in later round spermatids (Figure 3-5). Thus, high levels of *Ant4* expression are likely associated with entry of the male germ cells into meiosis. In contrast, the fraction enriching Sertoli cells expressed a very low level of *Ant4*. We also confirmed here, by real time RT-PCR, that the *Ant4* transcript is very low or undetectable in somatic organs and ovary. It should be noted here that, in contrast to a previous observation using a cryopreserved specimen (17), developing oocytes did not show any detectable Ant4 expression in paraffin-embedded formalin-fixed tissues (Figure 3-7). Using the same RNA samples prepared for the study above, we also investigated the expression pattern of the Ant2 gene in various organs and spermatogenic cell types (Figure 3-6). Of interest, the expression profile of *Ant2* in mice was reciprocal to that of *Ant4*. The *Ant2* transcript was high in somatic organs, but relatively low in whole testis and almost completely undetectable in testicular germ cells, except primitive spermatogonia.

Ant4 Function Within the Testis

We first sought to confidently determine the expression profile of Ant4. Following the elucidation of the expression pattern of Ant4 we extended our study to the investigation of its function.

Generation of Mice with a Targeted Disruption of Ant4

To investigate the i*n vivo* function of *Ant4*, we generated *Ant4*-deficient mice by homologous recombination in embryonic stem (ES) cells. The targeted disruption deleted exons 2 to 4, which encode amino acid residues 79-212 (Figure 3-8A). An IRES-ßgal cassette was inserted with a splicing acceptor site to allow for examination of the activity of the *Ant4* promoter. Disruption of the *Ant4* gene in mice was confirmed by Southern blot analysis (Figure 3-8B) and genomic PCR amplification (Figure 3-8C). Immunoblotting was used to confirm the absence of Ant4 protein expression in the *Ant4*-deficient mice as well as to analyze the levels of Ant1 and Ant2 (Figure 3-9). The relative protein levels of Ant2 in the $Ant4^{-/-}$ testis, when normalized by total protein amount, were increased in comparison to controls, whereas Ant2 levels were unaffected in heart. Interestingly, the levels of Ant2 as assayed by western blot were slightly increased in the testicular preparation of the Ant4-deficient mice. This inconsistency in the protein levels of Ant2 could be due to the increased somatic cell contribution as a proportion of the whole loaded protein. This would be the result of a higher somatic cell contribution in the Ant4-deficient testis due to the severely decreased germ cell component. Since Ant2 is ubiquitously expressed in most somatic tissues, the increased proportion of somatic tissue could explain this slight inconsistency in protein levels. The levels of Ant1 protein expression, which were high in heart and undetectable in testis, were unaffected by *Ant4* disruption. The *Ant4*-promoter-driven β-galactosidase expression from our targeted allele also enabled us to examine the *Ant4* expression profiles in mice. As expected, X-gal staining in $Ant4^{+/-}$ mice was observed

only in the testis but not in any other organs (data not shown). X-gal staining of the *Ant4*$^{+/-}$ testis demonstrated that the β-galactosidase activity was most clearly detectable when male germ cells transitioned into cells morphologically representative of spermatocytes (Figure 3-10), consistent with the immunohistochemistry data above.

Ant4 Deficient Mice Exhibit Impaired Spermatogenesis and Infertility

The *Ant4*$^{-/-}$ mice were viable and exhibited apparently normal development. The interbreeding of *Ant4*$^{+/-}$ mice produced offspring of normal litter size, and conformed to the Mendelian ratios of *Ant4*$^{+/+}$, *Ant4*$^{+/-}$ and *Ant4*$^{-/-}$ inheritance, 9, 27, and 13 respectively. In contrast to the similar body sizes between the wild type and mutant mice (data not shown), the testes of *Ant4*$^{-/-}$ adults were smaller than those of *Ant4*$^{+/+}$ adults (Figure 3-11). Testes from 6-week-old *Ant4*$^{-/-}$ males were approximately one-third the weight of those from control males. Closer examination of testicular development revealed similar growth patterns of the testis until approximately 17 days after birth, suggesting normal growth of the spermatogonia (Figure 3-13) (47). Subsequent development was impaired in *Ant4*$^{-/-}$ testis. Histological analysis of *Ant4*-deficient testis demonstrated clear morphological aberrations in the process of spermatogenesis as evident by the severe reduction of spermatocytes and vacuolization of the seminiferous epithelium (Figure 3-12). Furthermore, mating of *Ant4* deficient males with wild-type females did not produce any offspring. In contrast, *Ant4*$^{-/-}$ females were fertile and did not show any apparent ovarian abnormalities.

Ant4$^{-/-}$ Germ Cells Undergo Meiotic Arrest

To determine the stage at which *Ant4*$^{-/-}$ germ cells undergo arrest, RT-PCR analysis of transcripts present in different specific spermatogenic cell types was carried out (Figure 3-14). *Dazl*, which is expressed throughout spermatogenesis, was similarly expressed in the *Ant4*$^{+/+}$, *Ant4*$^{+/-}$, and *Ant4*$^{-/-}$ testis. The DNA mismatch repair gene *Dmc1*, which is expressed before the

pachytene spermatocyte stage (48, 49), did not exhibit significantly different expression patterns either. The expression of *A-Myb*, which is a transcription factor of the *Myb*-family that is expressed in type B spermatogonia and leptotene to pachytene spermatocytes (50), decreased in the *Ant4*$^{-/-}$ testis. The expression of *Dvl3*, which has been shown to be present from primitive type A spermatogonia through pachytene spermatocytes (51), also decreased in the *Ant4*$^{-/-}$ testis. Synaptonemal complex protein 3 (*Sycp3*), which is restricted to the zygotene to diplotene spermatocytes (52), was markedly decreased in the *Ant4*$^{-/-}$ testis. Transcripts normally present in pachytene spermatocytes and at later stages, such as *HoxA4* and *CyclinA1* (53,54), were not detected in the *Ant4*$^{-/-}$ testis. In addition, *Dvl1*, which is expressed in round, elongating, and elongated spermatids (51), was also undetectable in the *Ant4*$^{-/-}$ testis. These data indicate a decrease in meiotic, specifically at the stage of pachytene and beyond, and an absence of the postmeiotic germ cells in the *Ant4*$^{-/-}$ testis.

Ant4 Deficient Mice Possess a Decreased Number of Pachytene Spermatocytes and an Absence of Diplotene Spermatocytes

To further investigate the stage of Ant4-deficient spermatocytic arrest we utilized synaptonemal complex protein 3 (Sycp3) staining (Figure 3-15). Synaptonemal complex protein 3 (Sycp3) mediates the pairing and synapsis of homologous chromosomes during meiosis I and thus is utilized to demarcate the chromosomes. Upon analysis with Sycp3, the seminiferous epithelium of Ant4-deficient mice showed an increased proportion of leptotene like spermatocytes, as determined by the chromosomal condensation status of these cells. The Ant4-deficient spermatocytic compartment also contained zygotene and pachytene like cells, however the proportion of these cell types were decreased in comparison to controls.

In order to more precisely determine the stage of arrest of Ant4-deficient spermatogenic cells, we next performed a chromosomal spread analysis utilizing Sycp3, γH2AX and DAPI on

Ant4 wild-type (Figure 3-16) and Ant4-deficient (Figure 3-17) spermatocytes respectively. Phosphorylated H2AX (γH2AX) is a histone variant known to associate with double strand breaks. γH2AX is also known to associate with the chromosomes during meiosis I, specifically leptotene through diplotene of prophase I. γH2AX is implicated to have a role in conferring the heterochromatic transformation of the X and Y chromosomes that occurs during meiosis I. Sycp3 and γH2AX localization allowed us to determine exactly which stages of the meiotic prophase I were absent in the Ant4-deficient mice in comparison to controls. These data indicate a decrease in zygotene and pachytene spermatocytes with a complete absence of diplotene spermatocytes in Ant4-/- testes. We also found there to be a severe reduction in the percentage of pachytene spermatocytes (Figure 3-19). The overall number of pachytene spermatocytes were also severely decreased in comparison to controls (Figure 3-20). Utilizing γH2AX staining we investigated the affects of Ant4 deletion on sex body formation and XY inactivation which normally occur during meiosis I in the male germ cells. In the $Ant4^{-/-}$ spermatocytes there were abnormalities in both the localization of γH2AX and also the condensation status of the XY chromosomes during pachytene (Figures 3-17 and 3-18). These data indicate that Ant4 depletion leads to abnormalities in the formation of the sex body and in the proper inactivation of the X and Y chromosomes.

Ant4 Deficient Male Mice Exhibit Increased Levels of Apoptosis Within the Testis

TUNEL labeling and cleaved caspase-3 staining were utilized to analyze the apoptotic profile of adult (6 wks) *Ant4*$^{-/-}$ testis in comparison to controls (Figures 3-21 and 3-22). The testis of *Ant4*-deficient mice exhibited increased levels of TUNEL-positive cells within the seminiferous tubules as compared to controls (Figure 3-21). Upon closer examination, the majority of the TUNEL-positive cells within the seminiferous tubules of *Ant4*$^{-/-}$ mice appeared to

be spermatocytes based upon cellular morphology and position within the seminiferous epithelium (Figure 3-21 bottom panel). We also utilized caspase-3 staining within the testis to confirm the differential apoptotic profiles present between *Ant4*-deficient testis and controls (Figure 3-22). Taken together, these results suggest that the *Ant4*$^{-/-}$ testis contain a significantly higher number of apoptotic cells than controls, and the majority of these cells appear to be early spermatocytes. In order to investigate further the testicular development of *Ant4*$^{-/-}$ mice in comparison to controls, we utilized the synchronous nature of the first spermatogenic cycle in postnatal testes. Following birth, the testis undergo the first spermatogenic cycle which produces germ cells of advancing development with increasing age (47). Thus, the testis at 7 days postpartum contains only spermatogonia and somatic cells. At 12 days, leptotene and zygotene spermatocytes appear and by day 17 early pachytene spermatocytes are found. By day 22, more advanced pachytene spermatocytes and round spermatids are present, and by day 35, the complete complement of germ cells begins to be present (47). Around day 17, the *Ant4*$^{-/-}$ testis began to exhibit signs of increased cell death within the germ cell compartment (Figure 3-23). By day 22 clear morphological differences were present between *Ant4*$^{-/-}$ and control testes. These data further support our observation that in the *Ant4*$^{-/-}$ testis, the early spermatocytes begin to undergo changes indicative of cell death and that by the pachytene stage these spermatocytes undergo apoptosis.

Ant4 Promoter CpG Analysis

In order to investigate the role of methylation in the regulation of the adenine nucleotide translocase family of genes, we carried out a promoter CpG dinucleotide analysis. We utilized the MethPrimer program (http://www.urogene.org/methprimer/index1.html) to determine the presence or absence of promoter proximal CpG islands within the adenine nucleotide

translocases' genomic loci. We identified distinct CpG islands as calculated by MethPrimer within the Ant1, Ant2, and Ant4 promoter proximal regions.

Identification of CpG Islands at the Promoter Regions of Ant1, Ant2 and Ant4

In order to determine if *Ant1* and *Ant2*, similarly to *Ant4* were regulated in part by methylation we first investigated the promoter proximal regions of *Ant1*, *Ant2*, and *Ant4* for the presence of CpG rich areas known as CpG islands. The regions investigated extended 500 bp upstream of the predicted transcription initiation site and 212 bp downstream from the transcription initiation site extending into exon 1. Interestingly, this analysis revealed that like *Ant4*, *Ant1* and *Ant2* contained clearly discernable CpG islands within their promoter proximal regions (Figure 3-24).

Real-Time PCR Analysis of Ant1, Ant2 and Ant4 Transcript Levels in Various Tissues

For the purpose of our study it was necessary to determine the transcript levels of *Ant1*, *Ant2*, and *Ant4* in various tissues and to determine in which tissues each was expressed at its highest and lowest levels. In order to determine the transcript levels of each of *Ant1*, *Ant2* and *Ant4* we utilized Taqman™ real-time PCR analysis of RNA isolated from male mouse testis, kidney, heart, skeletal muscle, and tail, as well as RNA isolated from female tail. Each tissue was chosen carefully after searching the published data regarding the expression levels of Ant1, 2, and 4 in various tissues. The goal of the expression analysis was to determine the tissues in which each Ant was expressed at its highest and lowest levels. These data demonstrate that within the tissues analyzed, Ant1 is expressed most significantly in heart and skeletal muscle with the lowest transcript levels being present in liver; Ant2 is significantly expressed at the transcript level in kidney with the lowest levels being detectable in skeletal muscle or testis; and Ant4 is expressed most significantly in testis with the absence or very low levels of transcript being detectable in kidney (Figure 3-25).

Methylation Analysis of Ant1, Ant2, and An4 Promoter Proximal CpG's in Various Tissues

To investigate the methylation status of *Ant1*, *Ant2*, and *Ant4* in various mouse tissues we utilized combined bisulfite restriction analysis (COBRA). Using the restriction enzyme HhaI which digests DNA protected from bisulfite conversion by methylation at the sequence GCGC, we were able to quickly determine the methylation status of the promoter regions of *Ant1*, *Ant2*, and *Ant4* in various tissues. HhaI digestion of *Ant1*, *Ant2*, and *Ant4* promoter loci revealed an absence of methylation at the *Ant1* and *Ant2* promoter regions in all tissues analyzed, whereas *Ant4* exhibited the same methylation pattern as previously published (Figure 3-26) (Rodic et al.). Interestingly, Ant2 which is located on the X chromosome shows a partial methylation pattern in female tissue when analyzed by COBRA. The partial methylation of Ant2 in female tissue is most probably due to the random inactivation of one of the X chromosomes which occurs in females. In order to further probe the methylation status of *Ant1*, *Ant2*, and *Ant4* we utilized bisulfite sequencing analysis. Bisulfite analysis of promoter proximal CpG islands was carried out on selected tissues for *Ant1*, *Ant2*, and *Ant4*. We utilized the expression analysis to determine the tissues to be analyzed based on expression levels. For each of *Ant1*, *Ant2*, and *Ant4* we chose one tissue in which transcript levels were significantly present for each and also one in which little to no transcript was detectable. This allowed us to determine if there was any differential methylation status present between tissues in which these Ants were significantly expressed or not significantly expressed. To analyze the Ant1 promoter proximal CpG island methylation status we utilized heart as the expressing tissue and liver as the non-expressing tissue. For *Ant2* analysis we utilized kidney as the expressing tissue and skeletal muscle as the low expressing tissue, we also analyzed female tail to confirm our COBRA data for the partial methylation pattern present. For *Ant4* we utilized testis as the tissue expressing Ant4 and kidney as the tissue with little or no detectable expression. Bisulfite analysis confirmed our COBRA data

demonstrating no differential methylation analysis within tissues significantly expressing and not significantly expressing *Ant1*, and *Ant2* (Figure 3-27). Whereas Ant4 showed a differential methylation pattern between tissues in which it was significantly expressed and tissue in which the transcript was low to absent.

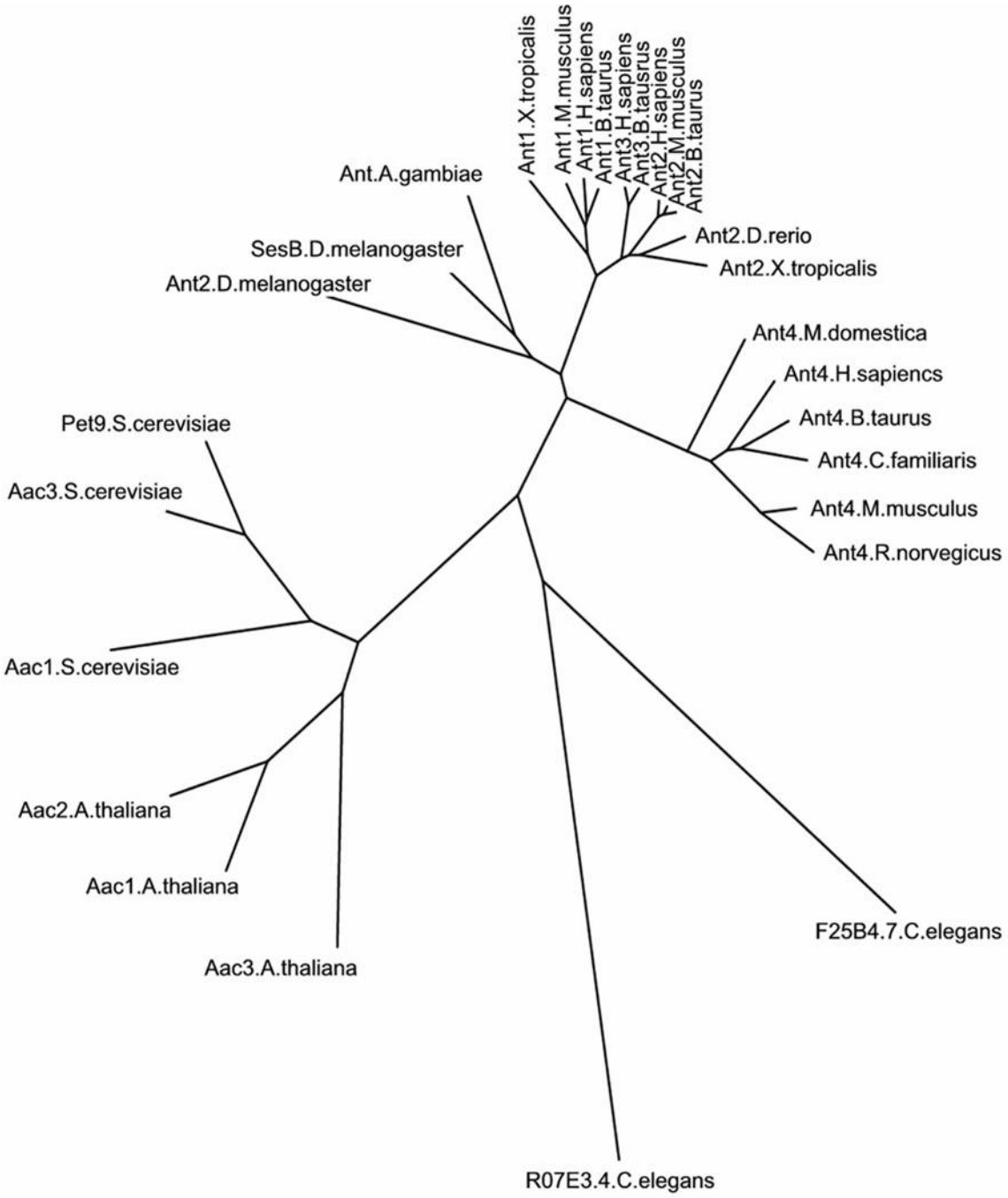

Figure 3-1. Phylogeny of ADP, ATP carrier proteins. A phylogram was generated using the ClustalW program (European Bioinformatics Institute). Ensembl gene IDs for Ant1, 2, 3, & 4 are shown in Table 1. Others include: Anopheles gambiae (ENSANGG00000017789), Drosophila melanogaster (CG16944, CG1683), Saccharomyces cerevisiae (YBL030C, YBR056W, YMR056C), Arabidopsis thaliana (NP_196853, NP_850541, NP_194568) and Caenorhabditis elegans (R07E3.4, F25B4.7).

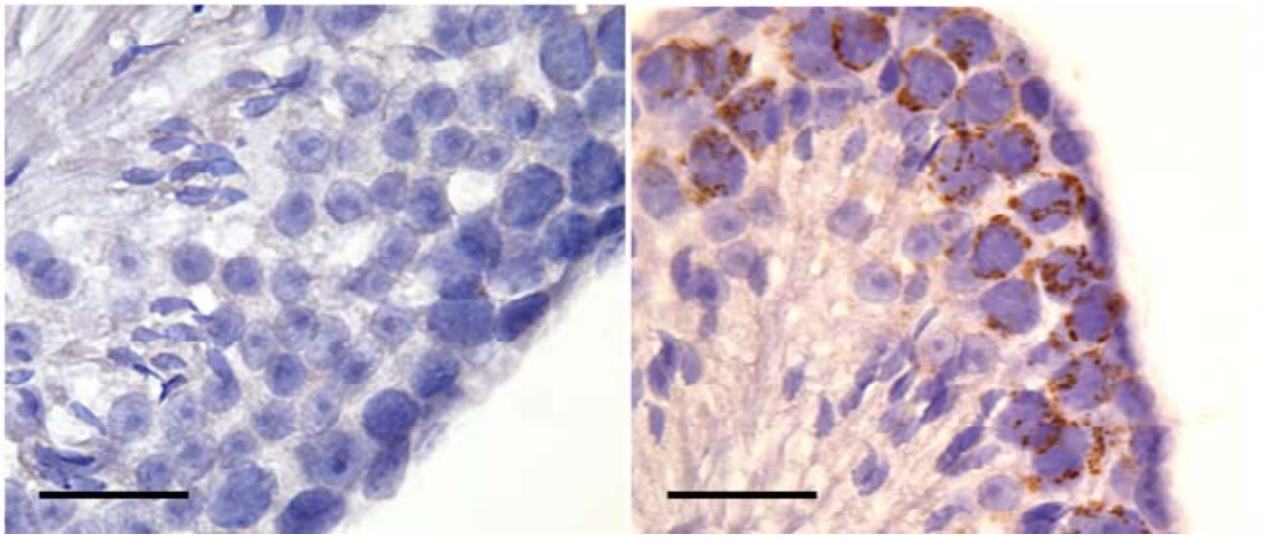

Figure 3-2. Ant4 expression is highest in mouse spermatocytes. (A) Immunohistochemical analysis of Ant4 expression in mouse testis: Paraffin-embedded sections of mouse testis from wild-type 6-week-old mice were incubated with a rabbit polyclonal antibody against mouse Ant4. Ant4 staining was visualized using DAB (brown), and slides were counterstained with hematoxylin. In control (top left), rabbit IgG was used as a primary antibody. Scale bars: 40 μm.

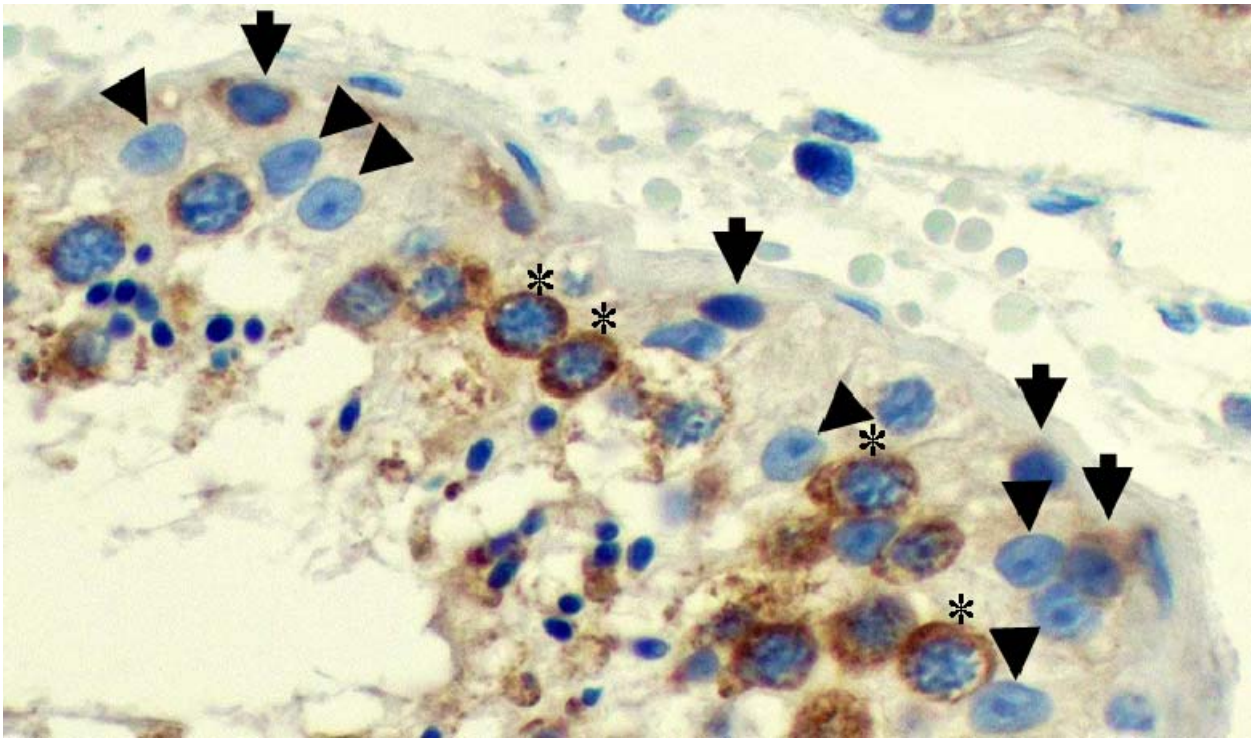

Figure 3-3. Ant4 expression is highest in human spermatocytes. (B) Immunohistochemical analysis of ANT4 expression in human testis: Formalin-fixed, paraffin-embedded sections of human testis from a 32 old male were incubated with a rabbit polyclonal antibody raised against human ANT4. ANT4 staining was visualized using DAB (brown), and slides were counterstained with hematoxylin. Arrows, arrowheads and asterisks indicate spermatogonia, Sertoli cells and spermatocytes, respectively. Scale bars: 50 μm.

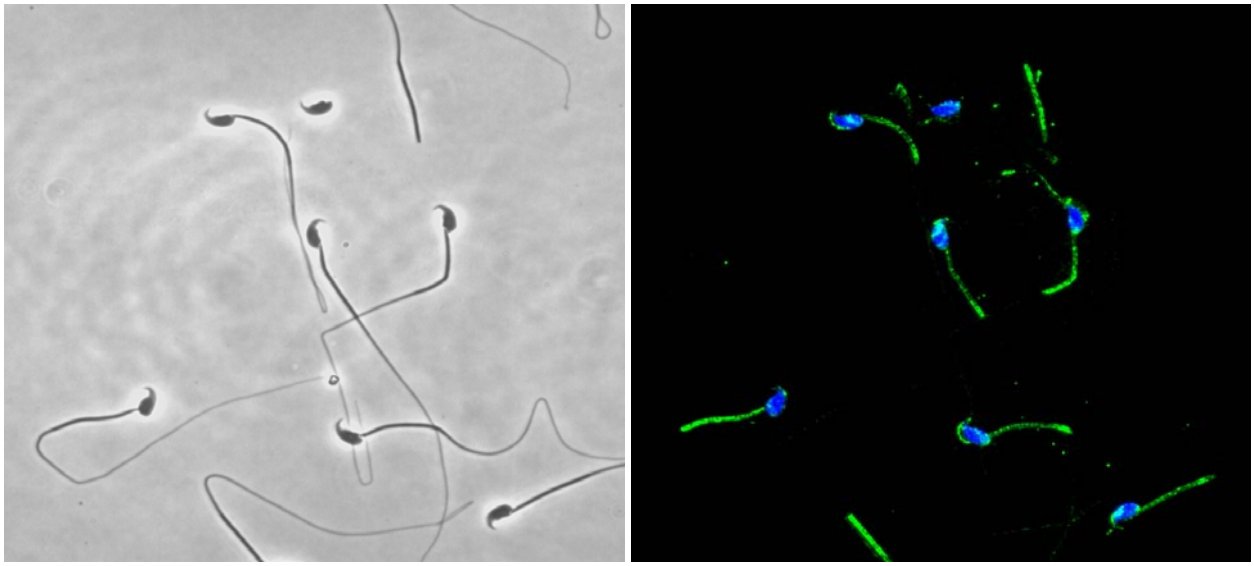

Figure 3-4. Ant4 is localized to the sperm midpiece. Left: Phase contrast microscopy of adult (6 weeks) mouse sperm isolated from the caudal epididymis. Right: Immunoflourescence of Ant4 expression in mouse sperm. Formaldehyde fixed, methanol permeablized sperm were incubated with the affinity-purified rabbit-anti mouse Ant4 antibodies at a concentration of 1:100. Alexa flour 488 conjugated goat-anti rabbit secondary antibodies were added at a 1:200 dilution. DAPI was added to slides and visualized using fluorescent microscopy. 60X magnification

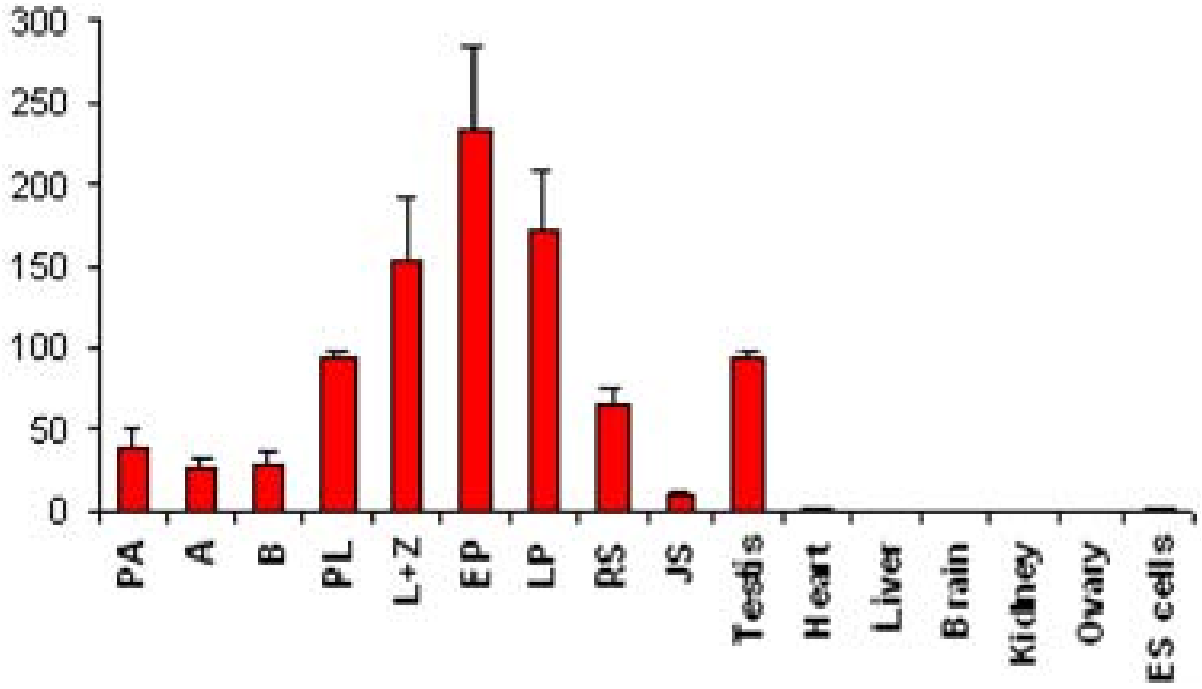

Figure 3-5. Ant4 peaks during meiosis I. TaqmanTM Real-time PCR analysis of Ant4 transcript levels in purified mouse spermatogenic cell types (PA = primitive type A spermatogonia, A = type A spermatogonia, B = type B spermatogonia, PL = preleptotene spermatocyes, L+Z = leptotene + zygotene spermatocytes, EP = early pachytene spermatocytes, LP = late or adult spermatocytes, RS= round spermatids, JS= juvenile sertoli cells) and various other tissues (whole testis, heart, liver, brain, kidney, ovary, and embryonic stem cells) (6week-old-mice). The relative transcript levels are shown in each graph when the transcript level of Ant4 in heart was set to 1.

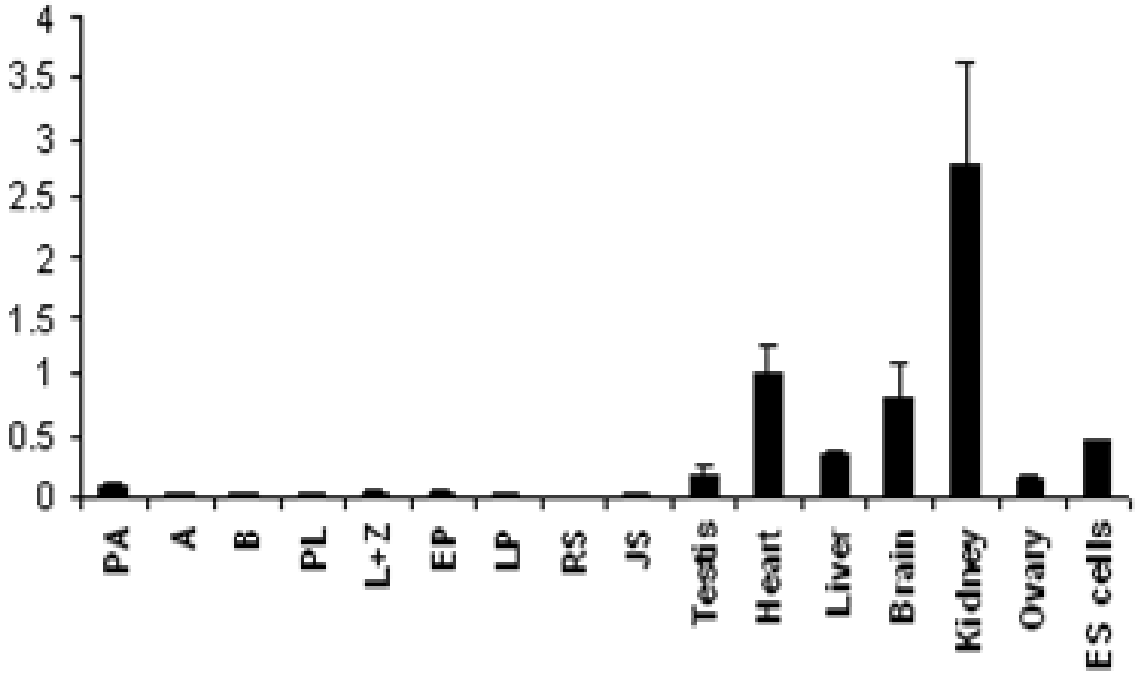

Figure 3-6. Ant2 levels are low to absent during meiosis I. TaqmanTM Real-time PCR analysis of Ant2 transcript levels in purified mouse spermatogenic cell types (PA = primitive type A spermatogonia, A = type A spermatogonia, B = type B spermatogonia, PL = preleptotene spermatocyes, L+Z = leptotene + zygotene spermatocytes, EP = early pachytene spermatocytes, LP = late or adult spermatocytes, RS= round spermatids, JS= juvenile sertoli cells) and various other tissues (whole testis, heart, liver, brain, kidney, ovary, and embryonic stem cells) (6week-old-mice). The relative transcript levels are shown in each graph when the transcript level of Ant2 in heart was set to 1.

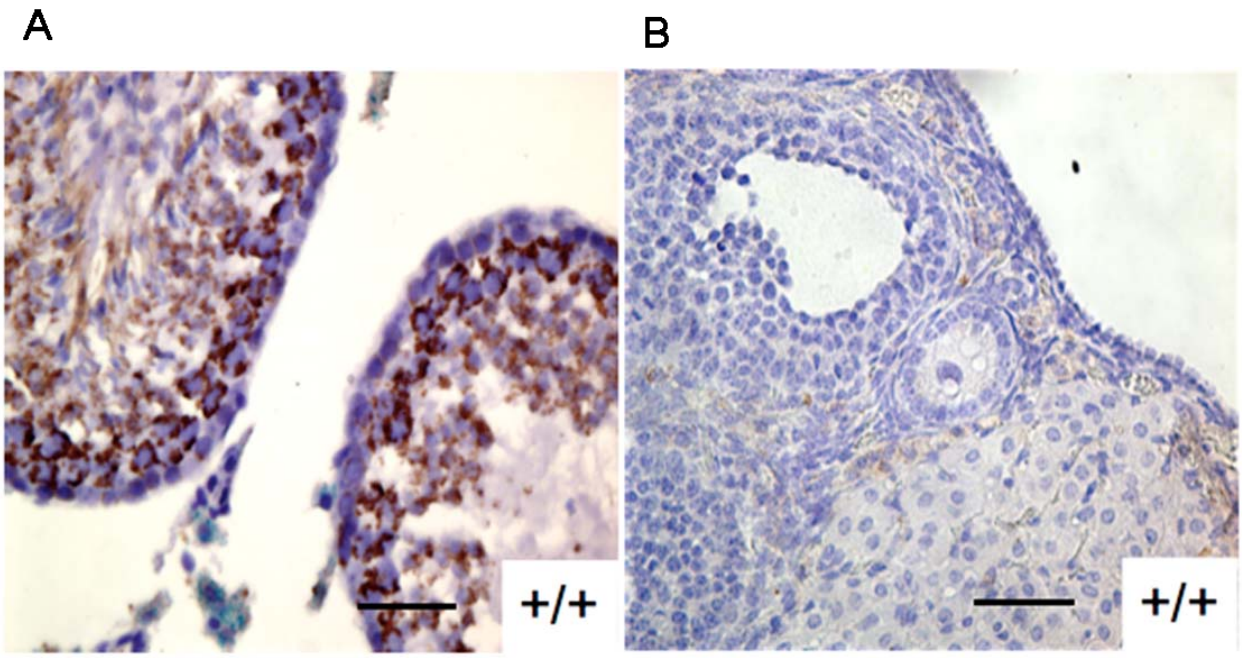

Figure 3-7. Histological analysis of Ant4 protein within the ovaries. Immunohistochemical analysis of paraffin-embedded sections of testes (A) and ovaries (B) from wild type (+/+) adult mice using a polyclonal antibody to Ant4.Scale Bars: 50μm. In contrast to a previous observation using a cryopreserved specimen (5), developing oocytes did not show any Ant4 expression. The present data are more consistent with real-time PCR analysis (Fig. 2C) and Northern blot analysis (5). Collectively, Ant4 expression appears to be low in ovaries including oocytes.

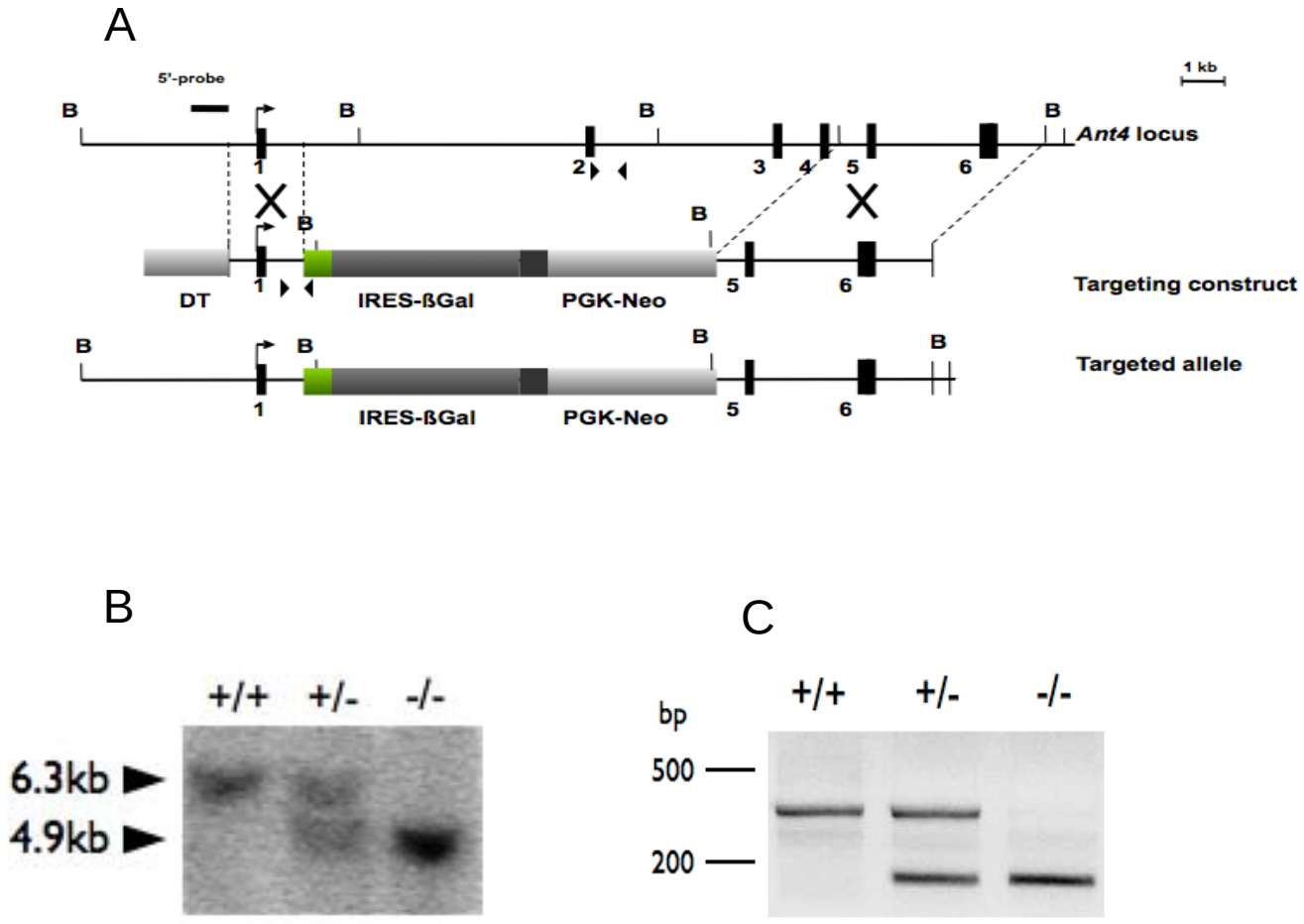

Figure 3-8. Gene targeting of *Ant4* (A) Strategy used for targeted disruption of the *Ant4* gene. (B) Southern blot analysis of BamHI-digested genomic DNA extracted from tails of wild-type (+/+), heterozygous (+/-) and homozygous (-/-) mutant mice. DNA was hybridized with the probe shown (5' external probe). (C) PCR analysis using allele-specific primers of genomic DNA of the indicated genotypes. Arrowheads in (A) denote the primers used for PCR amplification.

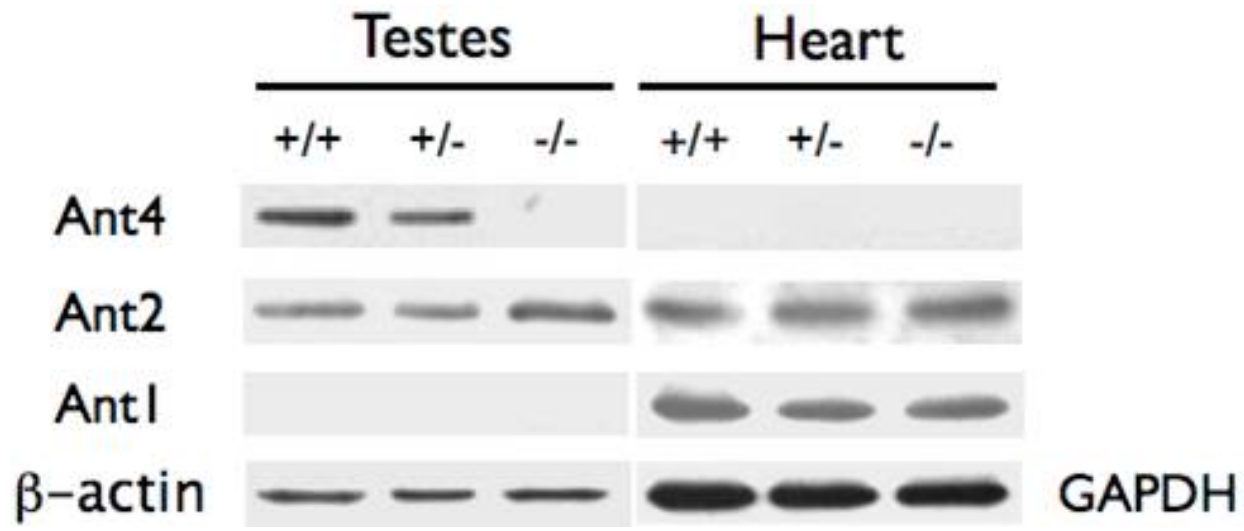

Figure 3-9. Confirmation of disrupted Ant4 Gene. Western blot analysis of Ant4 peptide expression as well as Ant1 and Ant2 in both testis and heart.

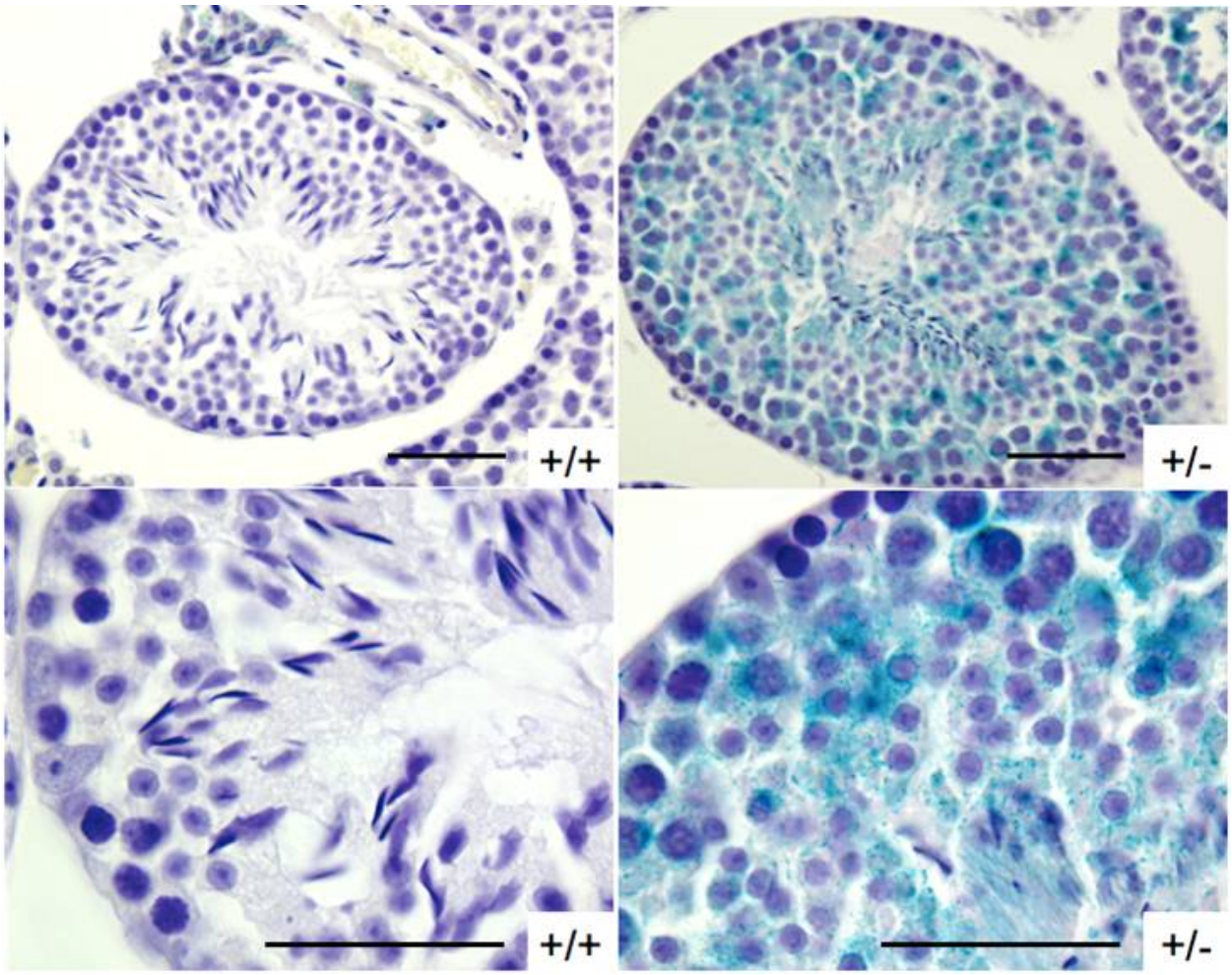

Figure 3-10. *Ant4* promoter-driven β-galactosidase expression pattern in testes. X-gal staining of wild-type (+/+, left panels), and heterozygous (+/-, right panels) testes, with low (top panels) and high (bottom panels) power magnification. *Ant4* promoter-driven β-galactosidase was not detected in spermatogonia or Sertoli cells, but was seen in primary spermatocytes and the subsequent cell types of spermatogenesis in heterozygous testes. Slides were counterstained with hematoxylin. Scale bars: 50 μm.

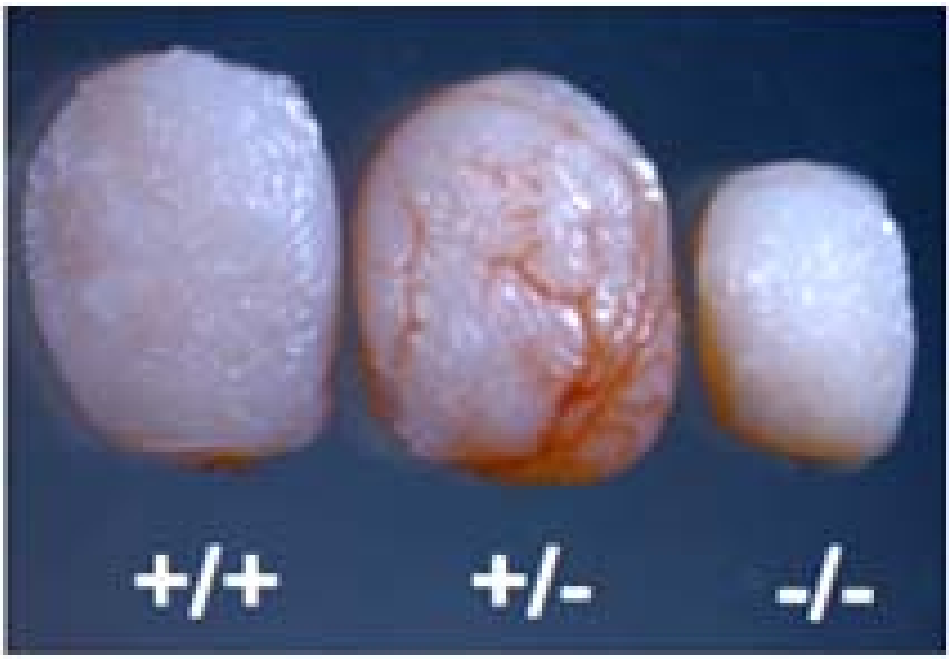

Figure 3-11. Severe reduction of testicular mass in Ant4-deficient mice. Gross morphology of testis from 6-week-old mice.

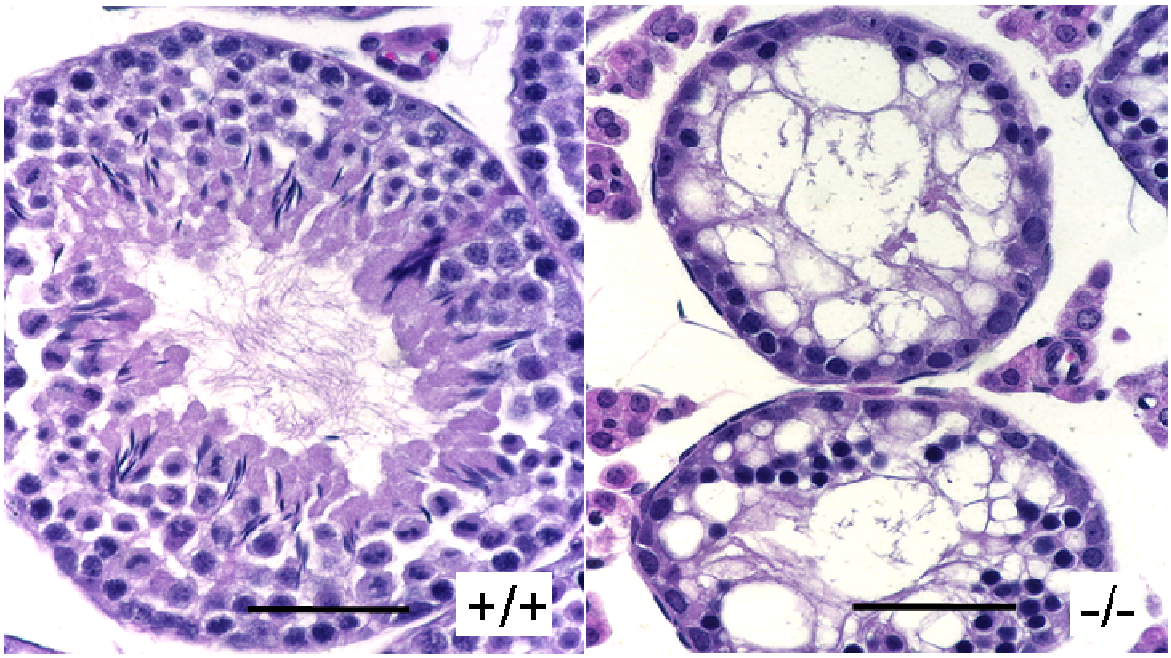

Figure 3-12. Ant4-deficient testis exhibit gross histological abnormalities. Histological analysis of testis (6-week-old) by hematoxylin and eosin staining. Scale bars: 50 μm.

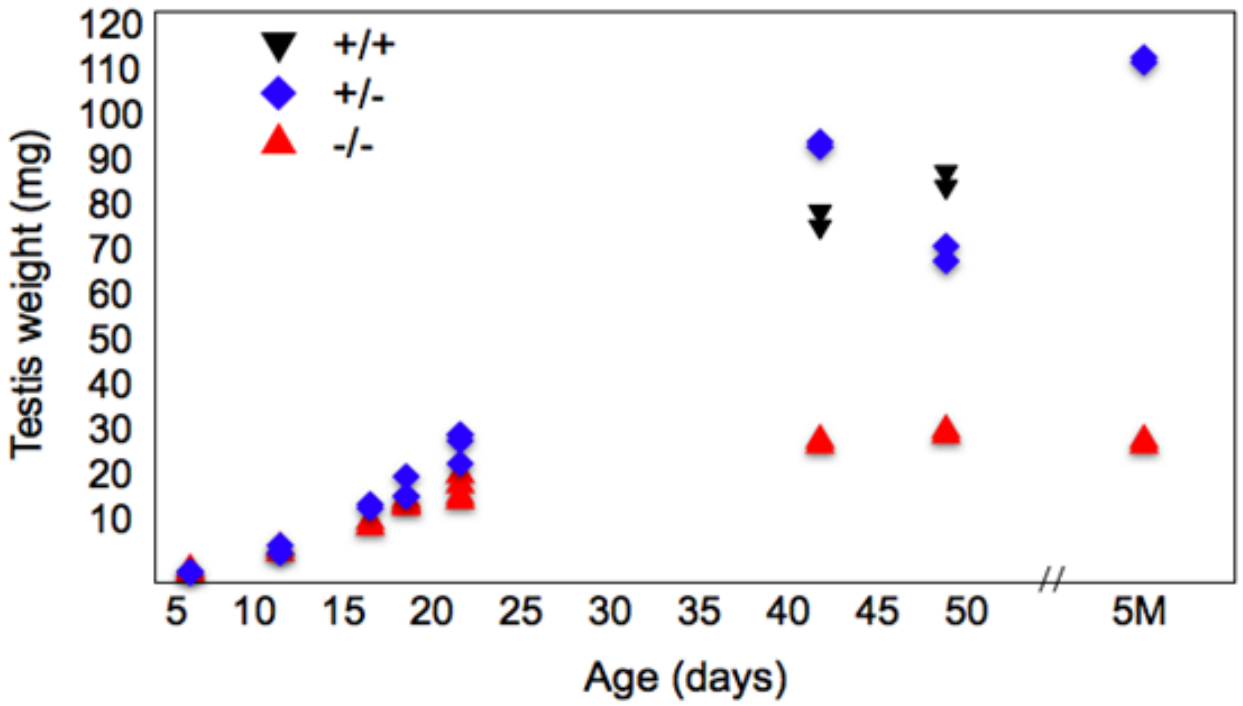

Figure 3-13. Testicular weight analysis. (A) Weight comparison of testis of the indicated genotypes (7 to 49 days old and 5 months).) (B) RT-PCR gene expression analysis in testis (6-week-old).

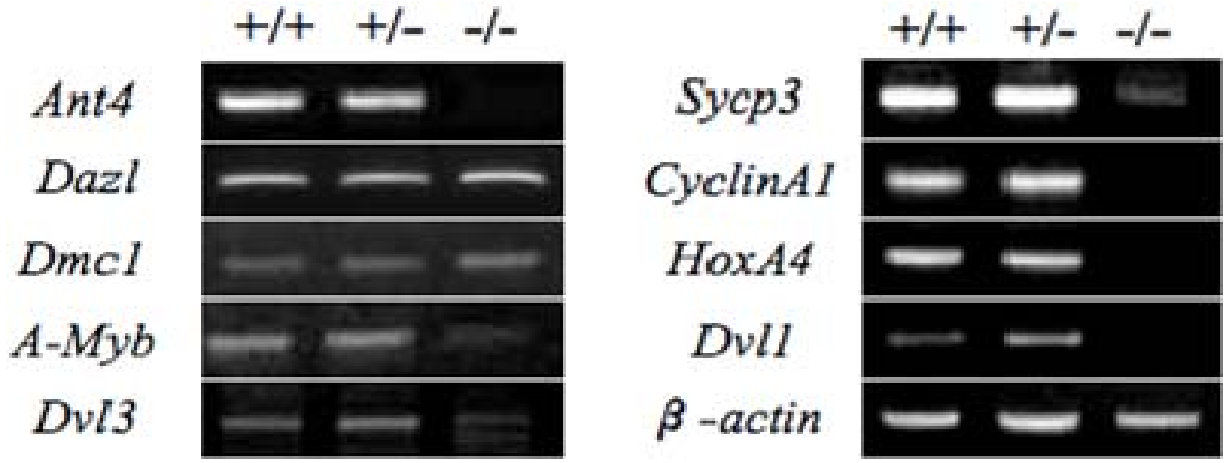

Figure 3-14. Transcript analysis of Ant-deficient testis. (A) Weight comparison of testis of the indicated genotypes (7 to 49 days old and 5 months).) (B) RT-PCR gene expression analysis in testis (6-week-old).

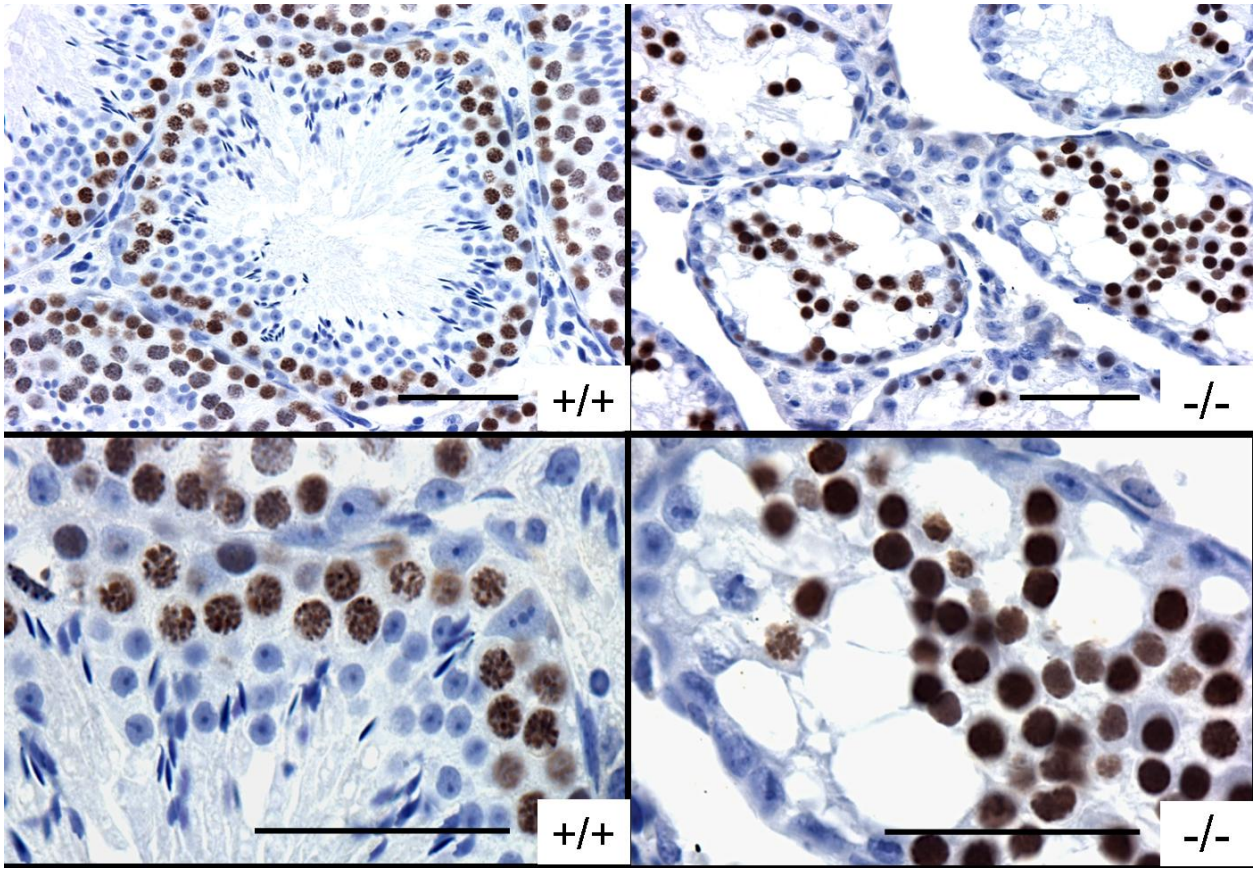

Figure 3-15. Sycp3 Chromosomal analysis. Immunohistochemical analysis of primary spermatocytes using Sycp3 staining in wild-type testis (left Panel) and in Ant4-deficient testis (right panel). Lower panels are high magnification images. Scale Bars: 50 µm.

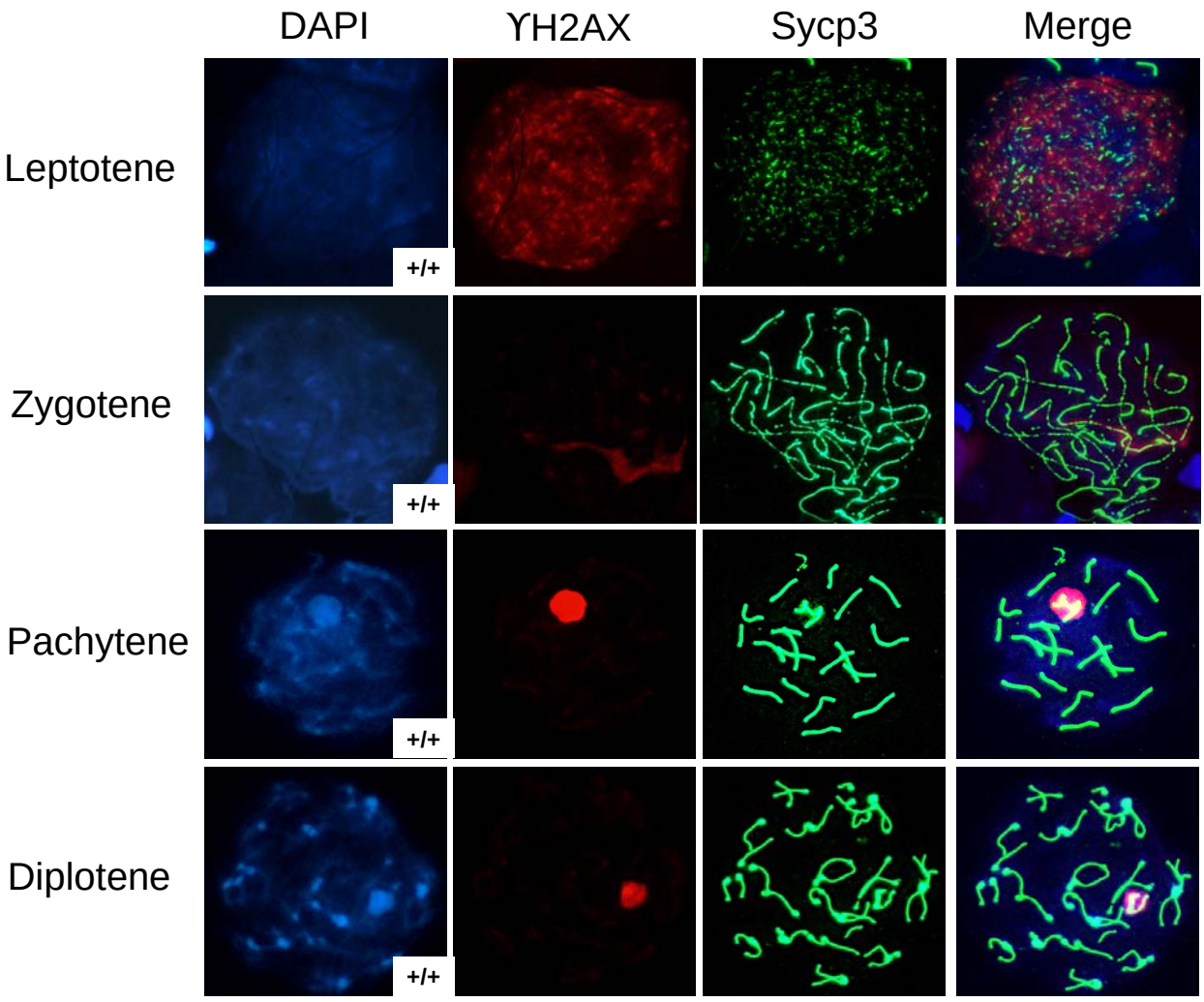

Figure 3-16. Ant4 wild-type spermatocytic chromosomal spread. Chromosomal spread analysis of freshly dissected testis from 6 week old wild-type mice. Spermatocytic preparations were incubated with both rabbit polyclonal Sycp3 and mouse monoclonal γH2AX at 1:200 dilutions. Sycp3 staining was visualized with an Alexa-fluor 488 conjugated anti-rabbit secondary antibody and γH2AX was visualized with a Cy3 conjugated anti-mouse secondary antibody.

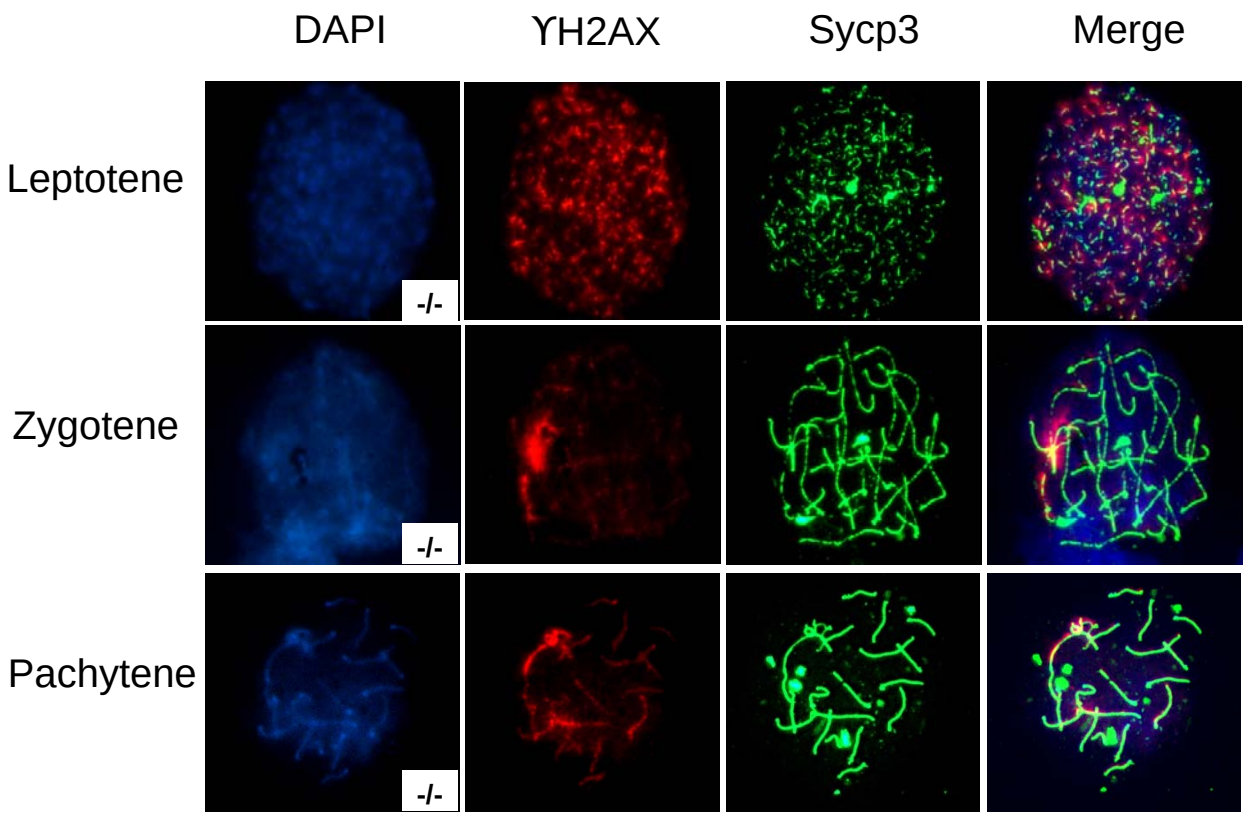

Figure 3-17. Ant4-deficient testis lack diplotene spermatocytes. Chromosomal spread analysis of freshly dissected testis from 6 week old Ant4-deficient mice. Spermatocytic preparations were incubated with both rabbit polyclonal Sycp3 and mouse monoclonal γH2AX at 1:200 dilutions. Sycp3 staining was visualized with an Alexa-fluor 488 conjugated anti-rabbit secondary antibody and γH2AX was visualized with a Cy3 conjugated anti-mouse secondary antibody.

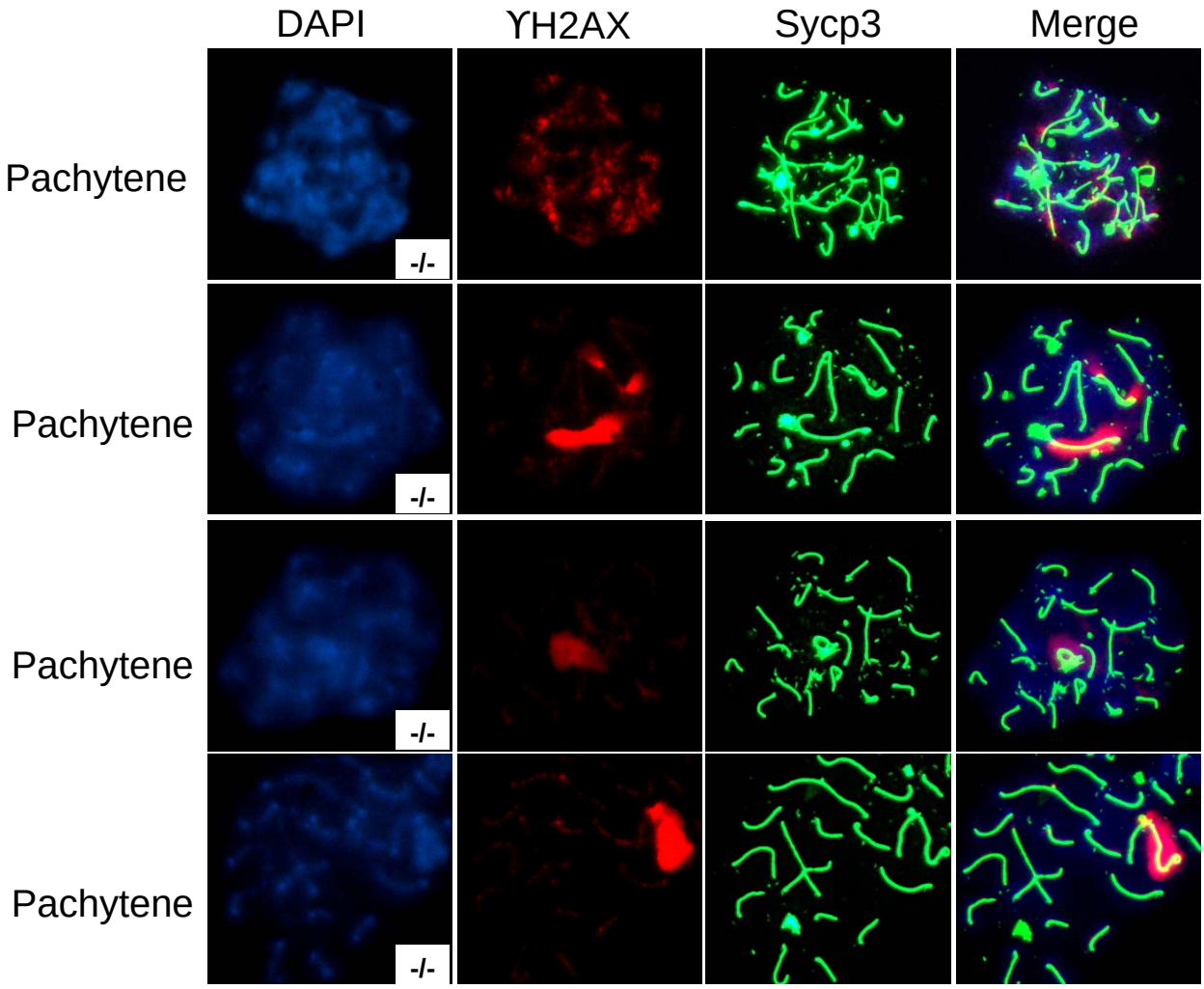

Figure 3-18. Pachytene abnormalities in Ant4-deficient spermatocytes. Chromosomal analysis of Ant4$^{-/-}$ pachytene spermatocytes utilizing Sycp3 and γH2AX staining. 60X magnification

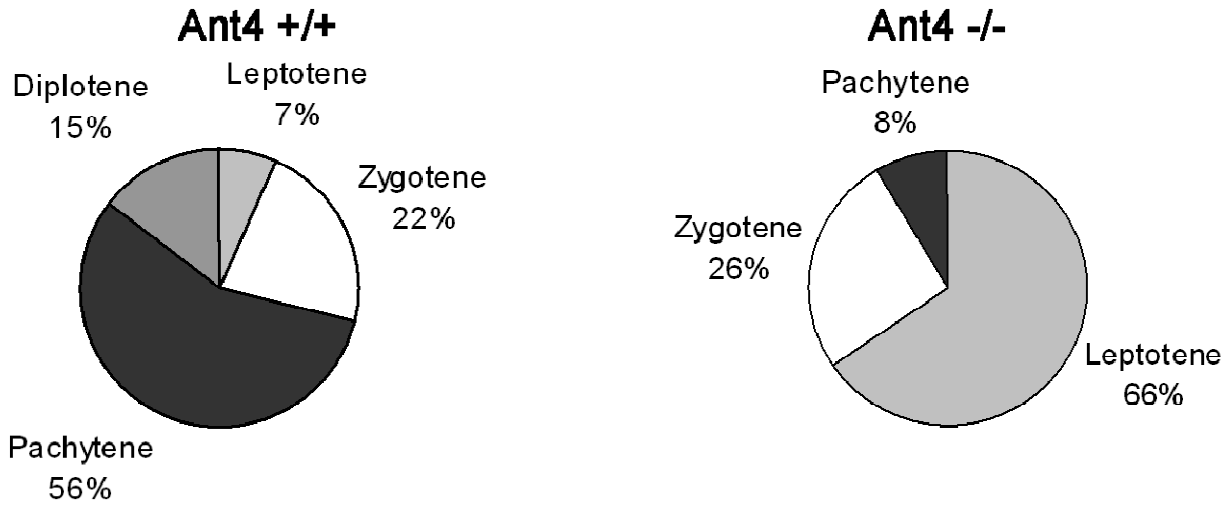

Figure 3-19. Quantification of spermatocytes in Ant4-deficient testis. Percentage analysis of the spermatocytic cells present in the seminiferous epithelium of Ant4 wild-type and Ant4-deficient testes.

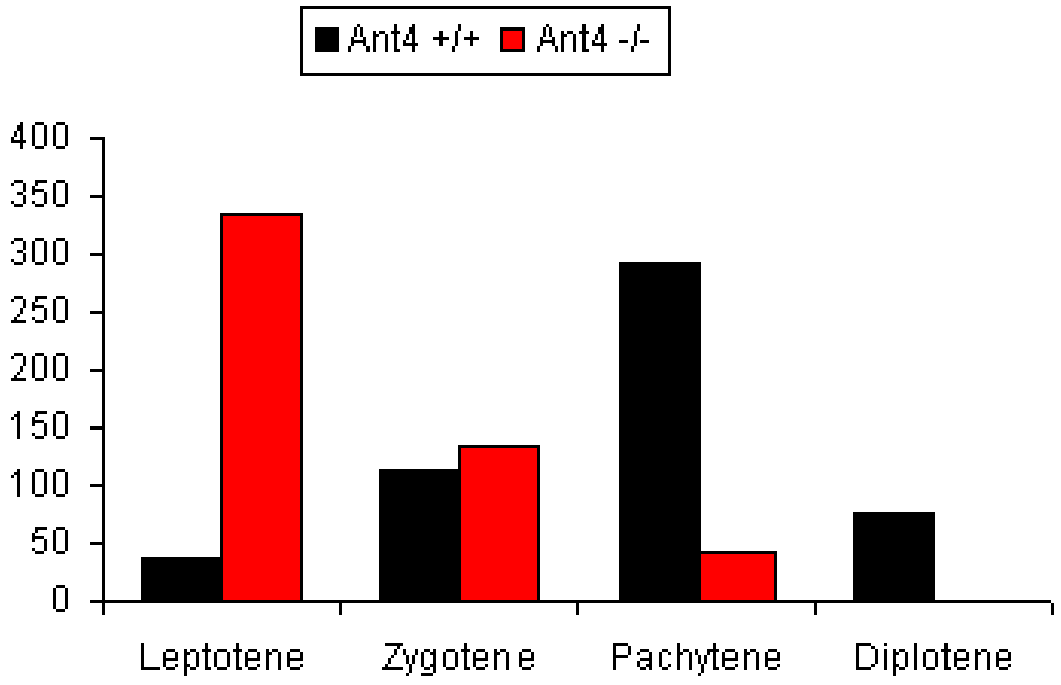

Figure 3-20. Spermatocyte counts. Quantification of spermatocytes, leptotene through diplotene of Ant4-deficient testis in comparison to controls.

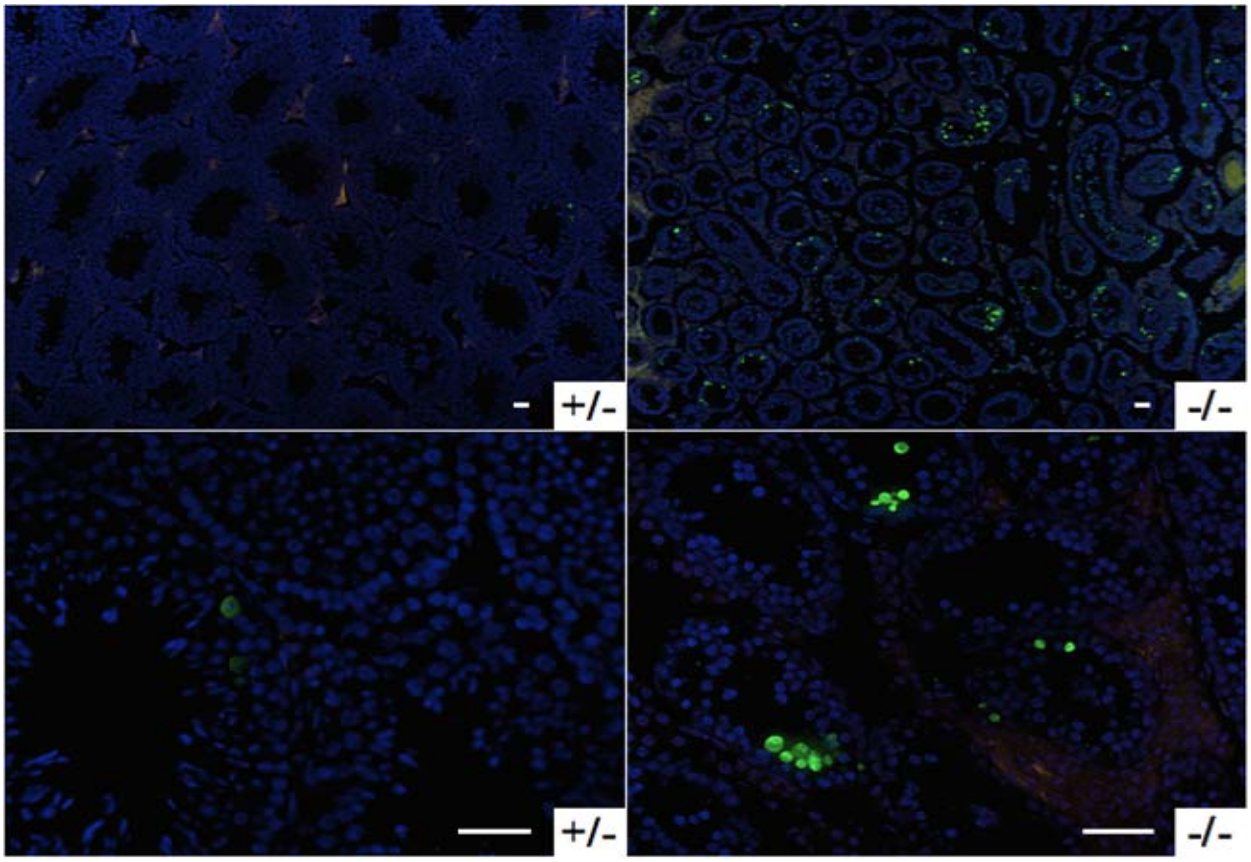

Figure 3-21. Apoptotic analysis of Ant4-deficient testis in comparison to controls. TUNEL analysis of Ant4 heterozygous mice (left panel) and Ant4-deficient testis (right panel). Lower panels are high magnification images. Scale Bars: 50µm

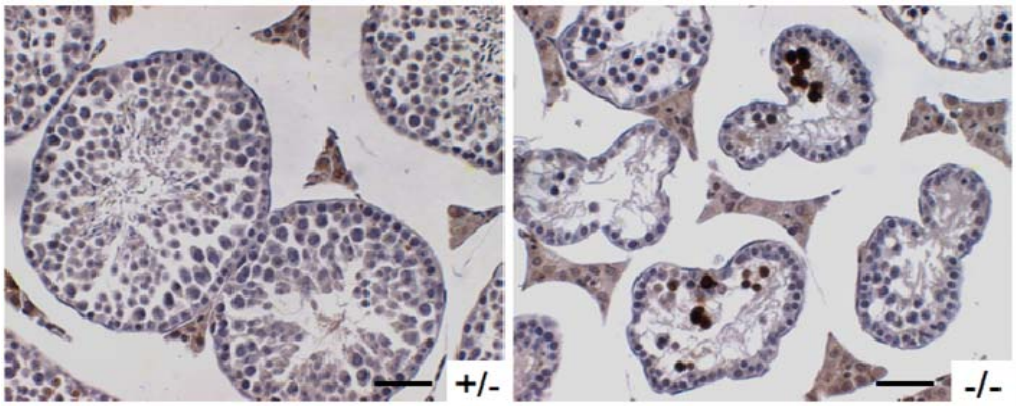

Figure 3-22. Cleaved Caspase-3 analysis. Immunohistochemical analysis of cleaved caspase-3 expression in testis from 6-week-old heterozygous mice (left), homozygous mutant mice (right). Cleaved caspase-3 staining was visualized using DAB (brown), and slides were counterstained with hematoxylin. Scale bars: 50 μm.

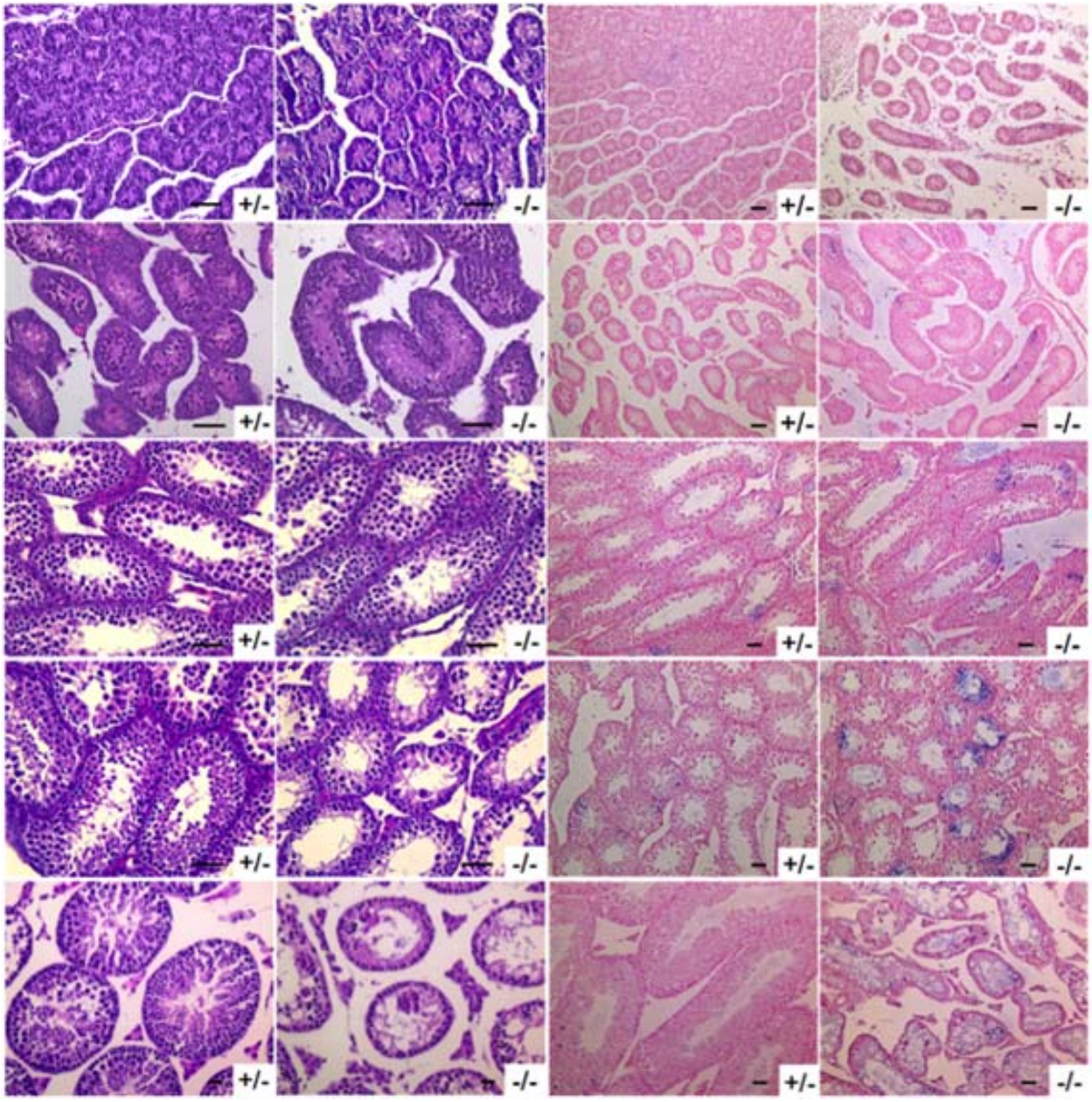

Figure 3-23. Postnatal development in the Ant4+/- and Ant4-/- testis. Left panels: Histological analysis (hematoxylin and eosin staining) of the testis during the first wave of spermatogenesis (D7-D22) and in the sexually mature adult, (D42) of heterozygous (+/-), and homozygous (-/-) mutant mice. Right panels: TUNEL analysis of the first wave of spermtogenesis (D7-D22) and in the adult, (D42) testis of heterozygous (+/-), and homozygous (-/-) mutant mice. Cells having DNA breaks were labeled using TdT and fluorescein-dUTP, and visualized using anti-fluorescein antibody conjugated with alkaline phosphatase (blue). Slides were counterstained with Nuclear Fast Red (pink).

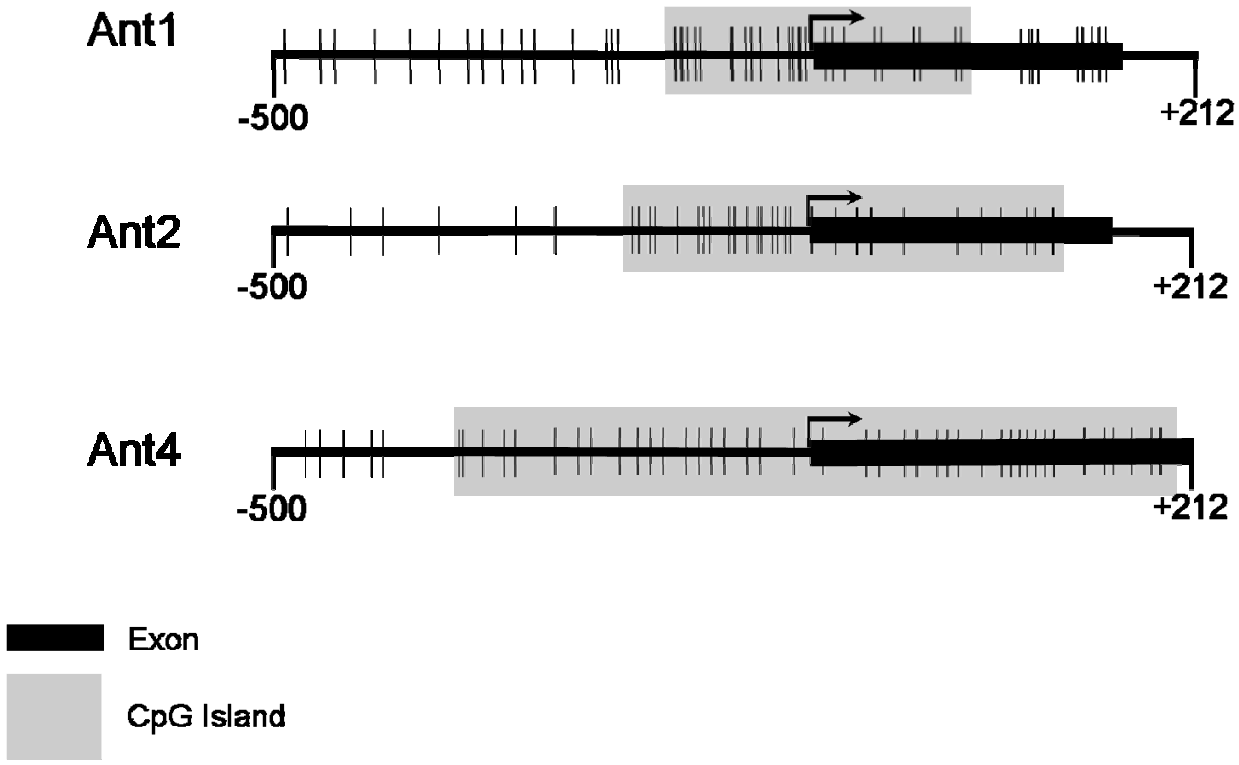

Figure 3-24. Adenine nucleotide translocase promoter analysis. Analysis of Ant1, Ant2, and Ant4 promoter proximal regions for the presence of CpG islands. The regions investigated extended 500 bp upstream of the predicted transcription initiation site and 212 bp downstream from the transcription initiation site extending into exon 1.

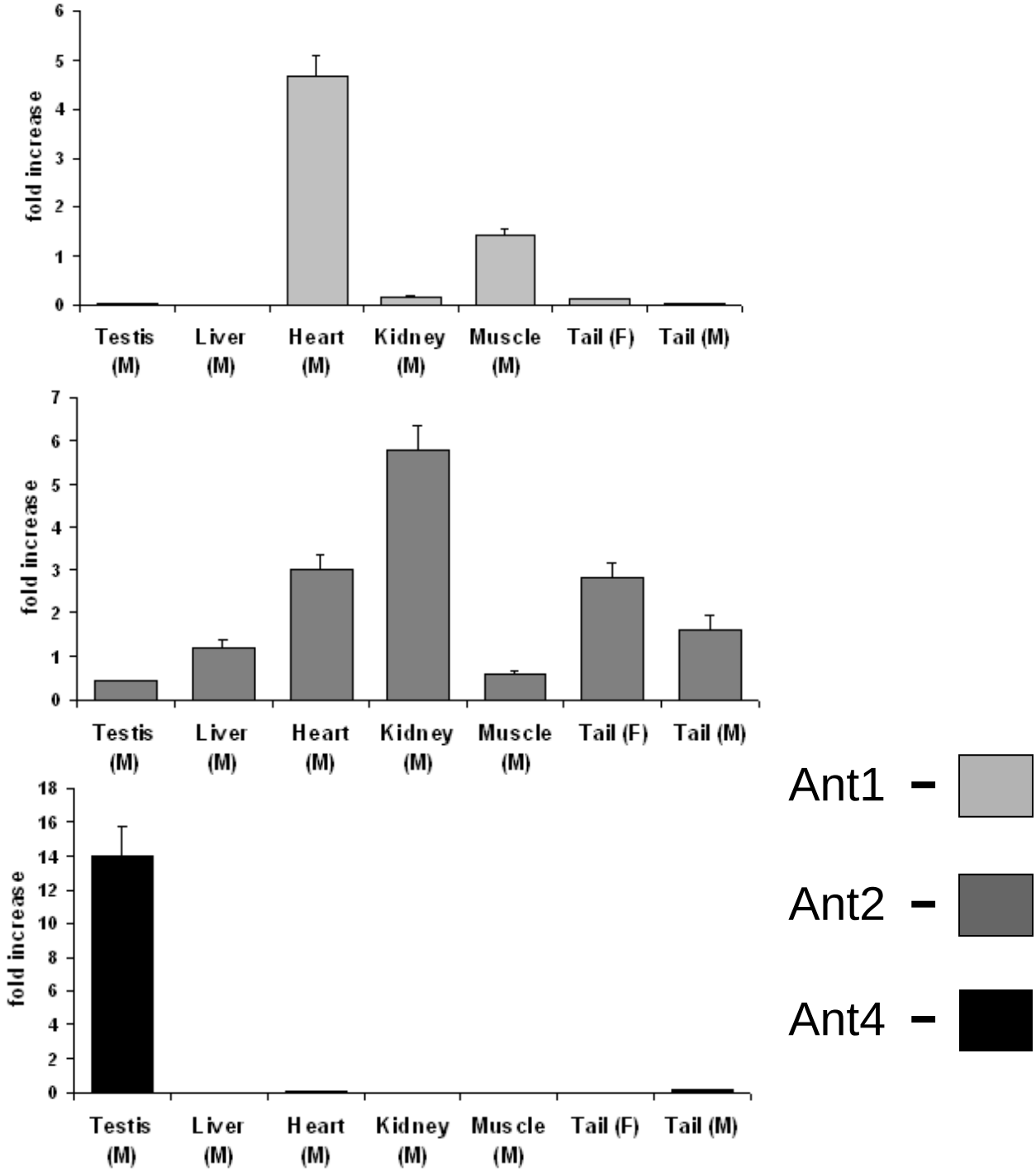

Figure 3-25. Ant1, Ant2, and Ant4 transcript level analysis in various tissues. Taqman™ Real-time PCR analysis of *Ant1*, *Ant2, and Ant4* transcript levels in testis, liver, heart, kidney, muscle, and male and female tail. Ant1:light gray, Ant2: dark gray, and Ant4: black.

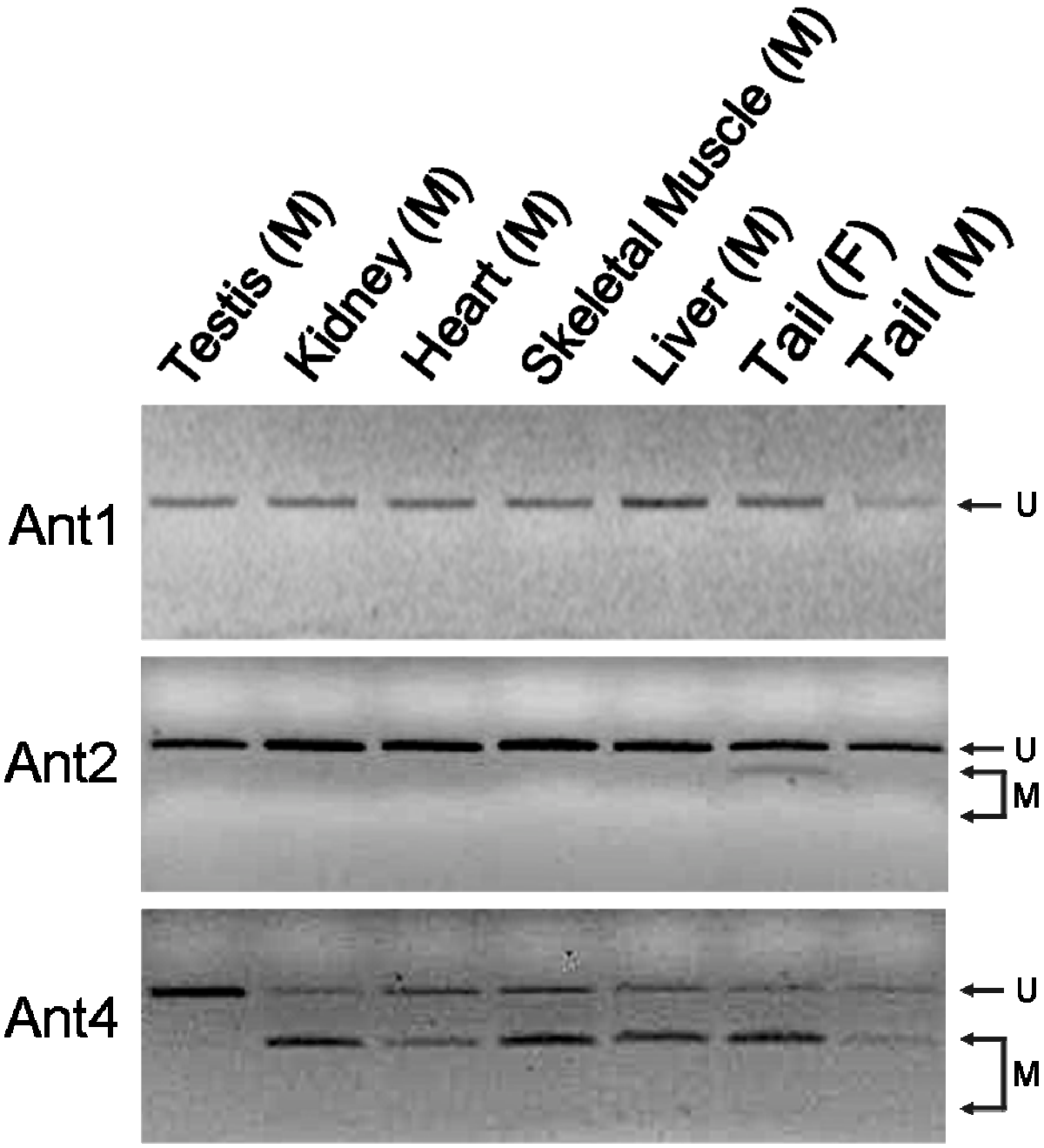

Figure 3-26. Combined Bisulfite Restriction analysis (COBRA) of Ant1, Ant2, and Ant4 promoter proximal CpG dinucleotides. Restriction analysis in testis, liver, heart, kidney, muscle, and male and female tail. U:unmethylated at restriction site, M:methylated at restriction site investigated.

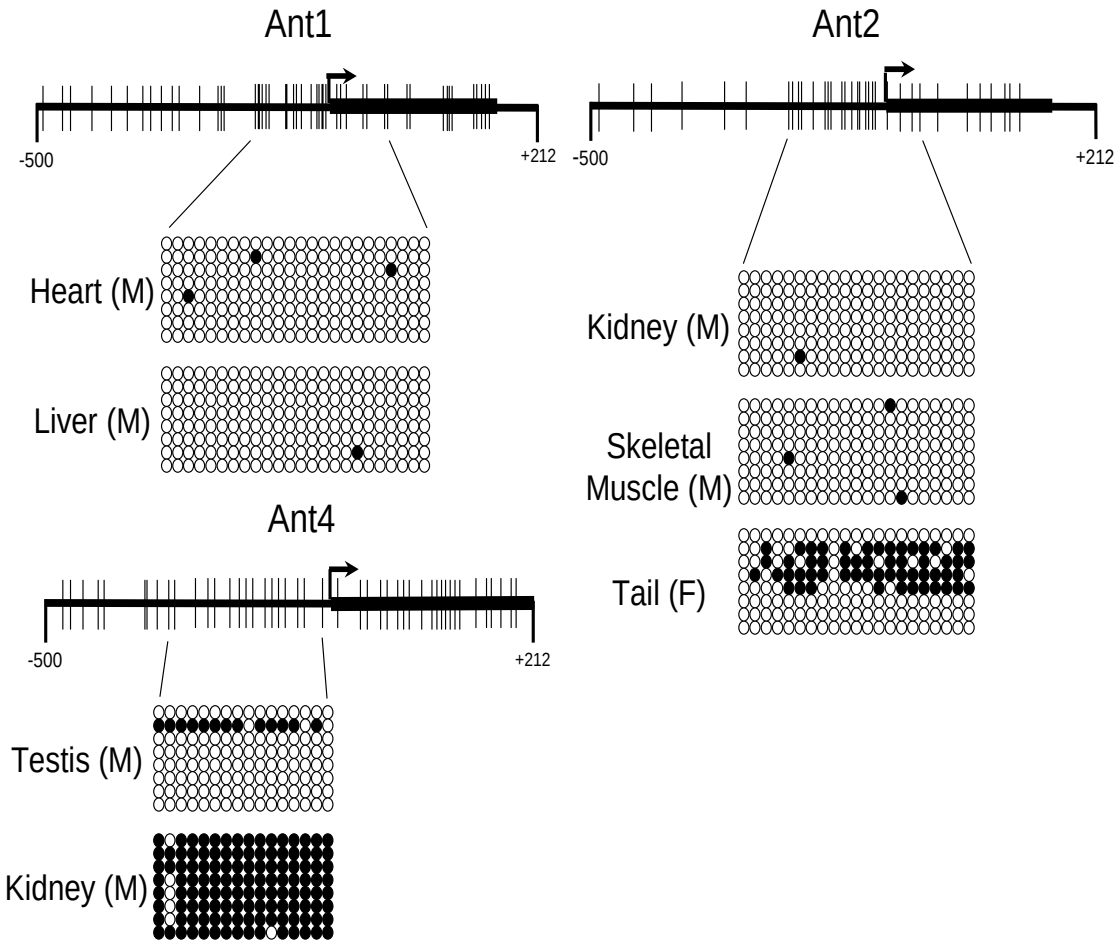

.

Figure 3-27. Bisulfite sequence analysis of Ant1, Ant2, and Ant4 promoter proximal CpG islands. Representative bisulfite analysis in various tissue types

	Ant1		Ant2		Ant4	
	Methylation status	E	Methylation status	E	Methylation status	E
Testes	○	-	○	+	○	++
Heart	○	++	○	+	●	-
Kidney	○	+	○	++	●	-
Muscle	○	++	○	+	●	-
Liver	○	-	○	+	●	-
Tail(F)	○	+	◑	+	●	-
Tail(M)	○	+	○	+	●	-

○ - unmethylated
● - methylated
◑ - mixture

E - expression level
++ high expression
+ intermediate
- low to absent

Figure 3-28. Methylation and expression correlation of Ant1, Ant2, and Ant4 in various tissues.

CHAPTER 4
DISCUSSION AND CONCLUSION

Spermatogenesis is the process by which self-renewing testicular precursors undergo proliferation, differentiation and maturation to produce viable spermatozoa. This process of spermatogenesis is one of the most elegant and complex examples of cellular growth and differentiation present within the mammalian system. Thus, there are many stages at which aberrations in spermatogenesis may lead to infertility. During the complex and energy demanding process of spermatogenesis the proliferating and differentiating spermatogenic cells rely on the production and availability of ATP from the mitochondria. Classically, aberrant mitochondrial function has been connected with deficient sperm motility. Reduced sperm motility has been reported in patients with mitochondrial diseases (55, 56), and pathogenic mutant mitochondrial DNA (mtDNA) has also been identified in semen samples of patients with fertility problems (57-59). However, a recent study revealed that the accumulation of mutant mitochondrial DNA in mice induced male infertility due to oligospermia and asthenozoospermia (60). Further, spermatogenic cells carrying >75-80% mutant mitochondrial DNA demonstrated meiotic arrest and displayed enhanced apoptosis, indicating that normal mitochondrial respiration is required for mammalian spermatogenesis as well as for sperm motility (60).

The present work has identified an essential role for the *Ant4* gene in mammalian spermatogenesis. The Ant4 gene is expressed exclusively during spermatogenesis both in mice and humans, while other Ants are utilized in somatic cells. Thus, Ant4 likely serves as the sole mitochondrial ADP/ATP carrier during spermatogenesis. Furthermore, without a functional ADP/ATP carrier protein ATP would not be efficiently transported into the cytosol, thus Ant4 is considered to be critical for normal spermatogenesis. Also, as a result of the absence of functional ADP/ATP translocation it might be inferred that inhibition of the electron transport

chain would occur. This inhibition would be due to the absence of a substrate for ATP production and also by the accumulation of ATP within the matrix of the mitochondria. The inhibition of the translocation of ADP/ATP would also result the production of high levels of reactive oxygen species due to the "leaking" of electrons form the 'backed-up" electron transport chain. Concomitant with the production of increased proportions of reactive oxygen species would also be the disruption of the electrochemical membrane potential of the mitochondria which might result in the depolarization of the membrane leading to apoptosis. Indeed, the disruption of the Ant4 gene resulted in meiotic arrest in mice as evidenced by the loss of meiotic and post-meiotic germ cells in the *Ant4*-deficient testis. The phenotype was similar to that seen in mice with aberrant mitochondrial DNA (60). Further, this loss appeared to result from an increase in apoptosis within the early spermatocyte population. This apoptosis led to the complete absence of diplotene spermatocytes and a severe reduction in the number of pachytene spermatocytes within the seminiferous epithelium of Ant4-deficient testis. Ant4-deficiency also resulted in the improper localization of γH2AX with the chromosomes and clear deficiencies in the heterochromatinization of the X and Y chromosomes. Although the exact Ant4 function of Ant4 within male germ cell mitochondria remains to be determined, the current study supports an idea that the ATP supply through normal oxidative respiration is critical for the processes of male germ cell meiosis.

Chromosomal locations of the Ant family genes are unique and conserved among mammalian species. The *Ant2* gene, which is ubiquitously expressed in somatic cells, is encoded by the X chromosome in all the mammalian species investigated. In mammalian males the X and Y chromosomes are known to undergo a heterochromatic transformation upon entry into meiosis, during prophase I, due to a lack of a homologous pairing partner (61-67). This

transformation, known as meiotic-sex chromosome inactivation (MSCI), confers transcriptional repression upon the X and Y chromosomes as demonstrated by RNA polymerase II exclusion (65, 66). On the other hand, the Ant4 gene, which apparently exists only in mammals, is always encoded on autosomes. These implicate a hypothesis that *Ant4* may have originally arose to compensate the loss of *Ant2* function during male meiosis. Female mammals have two X chromosomes and do not undergo MSCI (65, 66), which is consistent with the fact that *Ant4*-deficient female mice exhibit no observable decrease in fertility. Indeed, the *Ant2* and *Ant4* expression profiles were mutually reciprocal in the mice, and the *Ant2* expression was particularly low during spermatogenesis (Figure 3-6). Of interest, the expression of *Ant2* is very low not only in male meiotic germ cells but throughout spermatogenesis within the testis. Although the classical examples of MSCI show the repression of the genes after the pachytene stage, it is known that almost half of the X chromosome-linked genes are not expressed throughout spermatogenesis like the *Ant2* gene (65). After the emergence of *Ant4* in mammals, the expression of *Ant2* may have undergone further modifications to reduce transcription of the gene. In contrast to the low *Ant2* transcript levels in testicular germ cells, the overall Ant2 expression, both protein and mRNA, were more detectable in the whole testis preparation (Figures 3-6 and 3-9). This discrepancy may be due to a predominant expression of *Ant2* in somatic cells of the testis such as interstitial Leydig cells and vascular endothelial cells. However, we are currently unable to test this assumption because antibodies we had raised against Ant2 as well as any other available Ant2 antibodies do not work for immunohistochemistry.

Mammals have evolved a mechanism to compensate for the loss of gene expression from the sex chromosomes during male meiosis (46, 62, 64). Multiple autosomal retrogenes of X

chromosome origin have been reported as candidates potentially compensating for the absence of essential sex-linked gene expression during male meiosis, as exemplified by the *Pgk1*/*Pgk2* gene family (68-71). Although such retrogenes are considered to positively support male meiosis, there has been only one report so far (*Utp14b*) to clearly demonstrate the absolute necessity of such retrogenes in male meiosis (72, 73). It seems that even *Pgk2* null mice demonstrate minimal male infertility (depending on genetic background) mainly due to a sperm motility defect (74). In contrast, the present study demonstrates that the *Ant4* gene is essential for male meiosis. Indeed, the *Ant4* gene likely arose before the divergence of eutherian and metatherian lineages around the time when MSCI may have initiated (67). Thus, the *Ant* family of genes may be among the most essential to be compensated for during male meiosis. Interestingly, the *Ant4* gene is not a retrogene in contrast to all the other known potential autosomal "compensation" genes. This suggests that *Ant4* may have been generated by a standard gene duplication event in mammalian ancestors. It should be noted here that certain mammalian species including human, cow and dog but not rodents have another *Ant*, *Ant3* on the tip of the X chromosome (61,75). Human *ANT3* is encoded on Xp22 within the PAR1 region (40). This region is highly conserved between X and Y chromosomes, and is known to escape from sex chromosome inactivation during male meiosis (63, 65, 75). Thus, it would be plausible that some mammalian species may have evolved an additional protective mechanism to secure male meiosis. However, the role of *ANT3* in human spermatogenesis is questionable, considering the fact that *ANT3* expression is very low, just as *ANT2* expression, in human testis (http://symatlas.gnf.org/SymAtlas/).

An alternative hypothesis, not entirely exclusive of the above theory, is that the specification of the *Ant4* gene may have occurred in order to better support the process of spermatogenesis. Indeed, *Ant4* has distinguished N-terminus and C-terminus regions that are

conserved across mammalian species, which could potentially be adapted to a specific energy requiring process during male meiosis or subsequent sperm function. A recent report demonstrated that mitochondrial respiration defects due to the accumulation of mutated mitochondrial DNA lead to meiotic arrest and/or asthenozoospermia (60). This implies that male meiosis is one of the most energy demanding processes and is highly dependent on the production and availability of ATP from the mitochondria. It is possible that *Ant4* may have been altered during evolution in order to adjust to better fit such an energy demanding cellular environment. We believe this hypothesis to be more likely as demonstrated by our recent data. The improper localization of γH2AX and incomplete heterochromatinization of the X and Y chromosomes observed in the Ant4-deficient mice suggest that the X chromosome may not be completely silenced. Since it is quite clear that Ant4-deficiency results in improper condensation of the X and Y chromosomes, it is possible that Ant2 transcript could be produced off of the now slightly more euchromatic X. This would support the specialization theory of Ant4, in that the kinetics of Ant2 ADP/ATP exchange may not be best suited for the process of spermatogenesis. In addition, *ANT4* has been recently isolated from the fibrous sheath of the human sperm flagellar principal piece using mass spectrometry proteomics and was shown to co-localize with glycolytic enzymes (33). *Ant4* may have obtained an additional function which is advantageous for mammalian fertility regarding sperm function as well.

In summary, the present data demonstrate an essential role for *Ant4* in murine spermatogenesis, more particularly in the survival of meiotic male germ cells. We have clearly demonstrated that Ant4 deficiency results in the failure of the germ cells to progress through the essential process of meiosis. Specifically that Ant4 plays a crucial role during prophase I of meiosis I, and that in the absence of Ant4 there is a severe reduction in the number of pachytene

spermatocytes, with a complete absence of diplotene spermatocytes. Ant4-deficiency also results in the improper localization of γH2AX and aberrations in the heterochromatinization of the X and Y chromosomes, which normally occurs during prophase I. Additionally, this study demonstrates the molecular conservation of the *Ant* family of genes in mammals, and suggests a non-retrogene-based compensational mechanism of meiotic-sex chromosome inactivation in mammals.

This work has contributed a significant quantity of knowledge towards understanding the unique requirements of spermatogenesis, which have provided a solid foundation upon which to study male germ cell development. Approximately 15% of all couples are affected by infertility with half of all cases being attributed to the male (76). Due to the recent discovery of ANT4 there are currently no known clinical male infertility deficiencies related to ANT4. Our work in mouse has paved the way for the future discovery of any possible linkages of ANT4 to male infertility. Furthermore, despite currently available contraceptive methods, the world's population exceeds 6 billion and is currently increasing annually by approximately 80 million. These ever increasing numbers are resulting in overpopulation in many parts of the world leading to environmental destruction and a great deal of human suffering. Family-planning organizations estimate that much of this growth is unintended, indeed half of all conceptions are unplanned and half of the resulting pregnancies are undesired (77). This high rate of unintended pregnancy can be attributed to inadequate access to, or use of contraceptives, or both. Therefore, there is a significant need for a wider variety of contraceptive options in order to help control the high rate of unintended pregnancies. In particular developing alternative approaches for male based contraception could prove to be beneficial in decreasing the numbers of unwanted pregnancies. Currently male-directed contraception options are very limited, consisting of only condoms or

vasectomy. Despite this, men currently account for a third of all contraceptive use (78). Research into the development of a hormonal contraceptive for men analogous to the estrogen and progesterone pill used successfully by women has been undertaken and demonstrated to be effective in trials with most men, however, overall efficiency and efficacy is not yet as reliable as hormonal contraceptives in women (79). An alternative molecularly based male contraceptive with safety, efficacy, better cost-performance and less significant side effects would be highly beneficial. The appeal of a male contraceptive to men is widespread as in surveys, the majority of men indicate a willingness to utilize such a male contraceptive if available (80-82). Also approximately 98% of women in stable, monogamous, relationships would be willing to rely on their male partner to use such a method (80). Our work in characterizing a novel, testis specific adenine nucleotide translocase has provided a valuable foundation upon which to research the development of a male specific contraceptive. The future work will rely on our analysis and resultant phenotype of Ant4 disruption demonstrated here. The combination of our Ant4-deficient mouse model and the unique amino acid sequence and testis specific expression of Ant4 may prove to be ideal for the development of a male contraceptive and thus may contribute greatly to the future of contraception.

LIST OF REFERENCES

1. Henze, K., and Martin, W. (2003) *Nature* **426**, 127–128

2. Alberts, B., Johnson, A., Lewis, J., Raff, M., Roberts, K., and Walter, P. (2002) *Molecular Biology of the Cell. 4th Edition.* Garland Science

3. McBride, H.M., Neuspiel, and M., Wasiak, S. (2006) *Curr. Biol.* **16**, (14): 551

4. Alberts, B., Johnson, A., Lewis, J., Raff, M., Roberts, K., and Walter, P. (1994) *Molecular Biology of the Cell*. New York: Garland Publishing Inc

5. Herrmann, J.M., and Neupert, W. (2000) *Curr. Opin. Microbiol.* **3**, (2): 210–214

6. McMillin, J.B., and Dowhan, W. (2002) *Biochim. et Biophys. Acta.* **1585**, 97–107

7. Anderson, S., Bankier, A.T., Barrell, B.G., de Bruijn, M.H., and Coulson, A.R. (1981) *Nature* **410**, 141

8. Voet, D., Voet, J.G., and Pratt, C.W. (2006) *Fundamentals of Biochemistry, 2nd Edition*. John Wiley and Sons, Inc

9. Berg, J.M., Tymoczko, J.L., Stryer, L. (2002) *Biochemistry - 5th Edition*. WH Freeman and Company

10. Buchanan, J. (2000). *Biochemistry & molecular biology of plants*, 1st Edition, American society of plant physiology

11. Rich, P.R. (2003) *Biochem. Soc. Trans.* **31**, (6): 1095–105

12. Voet, D., and Voet, J.G. Biochemistry, 3rd Edition. John Wiley and Sons, Inc

13 Gawaz, M., Douglas, M.G., and Klingenberg, M. (1990) *J. Biol. Chem.* **265**, 14202-14208

14. Levy, S.E., Chen, Y., Graham, B.H., and Wallace D.C. (2002) *Gene* **254**, 57-66

15. Graham, B.H., Waymire, K.G., Cottrell, B., Trounce, I.A., MacGregor, G.R., and Wallace, D.C. (1997) *Nat. Genet.* **16**, 226-234

16. Dolce, V., Scarcia, P., Lacopetta, D., and Palmieri, F. (2005) *FEBS Lett.* **579**, 633-637

17. Rodic, N., Oka, M., Hamazaki, T., Murawski, M.R., Jorgensen, M., Maatouk, D.M., Resnick, J.L., Li, E., and Terada, N. (2005) *Stem Cells* **23**, 93-102

18. Fiore, C., Trézéguet, V., Le Saux, A., Roux, P., Schwimmer, C., Dianoux, A.C., Noél, F.,Lauquin, G.J., Brandolin, G., Vignais, P.V. (1998) *Biochimie* **80**, 137–150

19. Palmieri, L., Alberio, S., Pisano, I., Lodi, T., Meznaric-Petrusa, M., Zidar, J., Santoro, A., Scarsia, P., Fontanesi, F., Lamantea, E., Forrero, I., and Zebiani, M. (2005) *Hum. Mol. Genet.* **14**, 3079-3088

20. Santamaria, M., Lanave, C., and Saccone, C. *Gene* **333**, 51-59

21. Zoratti, M., and Szabo, I. (1995) *Biochim. Biophys. Acta.* **1241**, 139-76

22. Nicolli, A., Basso, E., Petronilli, V., Wenger, R.M., and Bernardi, P. (1996) *J. Biol. Chem.* **271**, 2185-92

23. Halestrap, A.P., Woodfield, K.Y., and Connem, C.P. (1997) *J. Biol. Chem.* **272**, 3346-54

24. Kokoszka, J.E., Waymire, K.G., Levy, S.E., Sligh, J.E., Cai, J., Jones, D.P., MacGregor, G.R., and Wallace, D.C. (2004) *Nature* **427**, 461-5

25. Hackenberg, H., and Klingenberg, M. (1980) *Biochemistry* **19**, 548–555

26. Stepien, G., Torroni, A., Chung, A.B., Hodge, J.A., and Wallace, D.C. (1992) *J. Biol. Chem.* **267**, 14592-7

27. Lunardi, J., Hurko, O., Engel, W.K., and Attardi, G. (1992) *J. Biol. Chem.* **267**, 15267-70

28. Ellison, J.W., Salido, E.C., and Shapiro, L.J. (1996) *Genomics* **36**, 369-71

29. Ceci, J.D. (1994) *Mamm. Genome* **5**, S124-38

30. Hirano, M., and DiMauro, S. (2001) *Nephrology* **57**, 2163-216

31. Van Goethem, G., Dermaut, B., Lofgren, A., Martin, J.J., and Van Broeckhoven, C. (2001) *Nat. Genetics* **28**, 211-212

32. Lodi, T., Bove, C., Fontanesi, F., Viola, A.M., and Ferrero, I. (2006) *Biochem. Biophys. Res. Commun.* **341**, 810-5

33. Kim, Y.H., Haidl, G., Schaefer, M., Egner, U., and Herr, J.C. (2007) *Dev. Biol.* **302**, 463-476

34. Belzacq, A.S., Vieira, H.L., Kroemer, G., and Brenner, C. (2002) *Biochimie* **84**, 167-176

35. Heller, C.G.; Clermont, Y. (1963) *Science* **140**, (3563): 184-6

36. Hess, R.A. (1999) *Encyclopedia of Reproduction*, *Volume 4.* Academic Press

37. Chiarini-Garcia, H., Raymer, A.M., Russel, L.D. (2003) *Reproduction* **126,** 669-680

38. Principles of Genetics, Fourth Edition, John Wiley and Sons, Inc., 2006

39. Raven, P.H., Johnson, G.B., Mason, K.A., Losos, J., and Singer, S. (2007) Biology, Eighth Edition, McGraw-Hill

40. Petronczki, Mark; Siomos, Maria F. & Nasmyth, Kim (2003) *Cell* **112** (4): 423-40

41. Griffiths, A.J.F., Wessler, S.R., Lewontin, R.C., Gelbart, W.M., Suzuki, D.T., and Miller, J.H. (2005) Introduction to Genetic Analysis, Eighth Edition, W.H. Freeman and Company

42. Xiong, X., Wang, A., Liu, G., Liu, H., Wang, C., Xia, T., Chen, X., and Yang, K. (2006) *Environ. Res.* **101** (3): 334-9

43. Sofikitis, N., Giotitisas, N., Tsounapi, P., Baltogiannis, D., Giannakis, D., and Pardalidis, N. (2008) *J. Steroid Biochem. Mol. Biol. In Press*

44. McCarrey, J.R., and Thomas, K. (1987) Nature **326**, 501-505

45. Kawasome, H., Papst, P., Webb, S., Keller, G.M., Johnson, G.L., Gelfand, E.W., and Terada, N. (1998) *Proc. Natl. Acad. Sci. USA.* **95**, 5033-5038

46. Wang, P.J. (2004) *Trends Endocrinol. Metab.* **15**, 79-83

47. Richardson, L.L., Pedigo, C., and Handel, M.A. (2000) Biol. Reprod. **62**, 789-79

48. Habu, T., Taki, T., West, A., Nishimune, Y., and Morita, T. (1996) *Nucleic Acids Res.* **24**, 470-477

49. Kuramochi-Miyagawa, S., Kimura, T., Ijiri, T.W., Isobe, T., Asada, N., Fujita, Y., Ikawa, M., Iwai, N., Okabe, M. Deng, W., Lin, H., Matsuda, and Y., Nakano, T. (2004) *Development* **131**, 839-849

50. Mettus, R.V., Litvin, J., Wali, A., Toscani, A., Latham, K., Hatton, K., and Reddy, E.P. (1994) *Oncogene* **9**, 3077-3086

51. Guo, R., Yu, Z., Guan, J., Ge, Y., Ma, J., Li, S., Wang, S., Xue, S., and Han, D. (2004) *Mol. Repro. Devel.* **67**, 264-272

52. Meuwissen, R.L., Offenberg, H.H., Dietrich, A.J., Risewijk, A., van Iersel, M., and Heyting, C. (1992) *EMBO J.* **11**, 5091-5100

53. Rubin, M., Toth, L.E., Patel, M.D., D'Eustachio, P., and Nguyen-Huu, M.C. (1986) *Science* **233**, 663-667

54. Sweeney, C., Murphy, M., Kubelka, M., Ravnik, S.E., Hawkins, C.F., Wolgemuth, D.J., and Carrington, M. (1996) *Development* **122**, 53-64

55. Folgero, T., Bertheussen, K., Lindal, S., Torberqsen, and T., Oian, P. (1993) *Hum. Reprod.* **8**, 1863-1868

56. Spiropoulos, J., Turnbull, D.M., and Chinnery, P.F. (2002) *Mol. Hum. Reprod.* **8**, 719-721

57. Kao, S., Chao, H.T., and Wei, Y.H. (1995) *Biol. Reprod.* **52**, 729-736

58. Lestienne, P., Reynier, P., Chretien, M.F., Penisson-Besnier, I., Malthiery, Y., and Rohmer, V. (1997) *Mol. Hum. Reprod.* **3**, 811-814

59. Carra, E., Sanqiorqi, D., Gattuccio, F., and Rinaldi, A.M. (2004) *Biochem. Biophys. Res. Commun.* **10**, 333-339

60. Nakada, K., Sato, A., Yoshida, K., Morita, T., Tanaka, H., Inoue, S., Yonekawa, H., and Hayashi, J. (2006) *Proc. Natl. Acad. Sci. USA.* **103**, 15148-53

61. Charchar, F.J., Svartman, M., El-Mogharbel, N., Venture, M., Kirby, P., Matarazzo, M.R., Ciccodicola, A., Rocchi, M., D'Esposito, M., and Graves, J.A.M. (2003) *Genome Res.* **13**, 281-286

62. Emerson, J.J., Kaessmann, H., Betran, E., and Long, M. (2004) *Science* **303**, 537-540

63. Fernandez-Capetillo, O., Mahadevaiah, S.K., Celeste, A., Romanienko, P.J., Camerini-Otero, R.D., Bonner, W.M., Manova, K., Burgoyne, P., and Nussenzweig, A. (2003) *Dev. Cell* **4**, 497-508

64. Graves, J.A.M. (2006) *Cell* **124**, 901-914

65. Khalil, A.M., Boyar, F.Z., and Driscoll, D.J. (2004) *Proc. Natl. Acad. Sci. USA.* **101**, 16583-16587

66. Namekawa, S.H., Park, P.J., Zhang, L., Shima, J.E., McCarrey, J.R., Griswold, M.D., and Lee, J.T. (2006) *Curr. Biol.* **16**, 660-667

67. Turner, J.M.A., Mahadevaiah, S.K., Ellis, P.J.I., Mitchell, M.J., and Burgoyne, P.S. (2006) *Dev. Cell* **10**, 521-529

68. Chen, K., Knorr, C., Moser, G., Gatphayak, K., and Brenig, B. (2004) *Mamm. Genome* **15**, 996-1006

69. Erickson, R.P., Kramer, J.M., Rittenhouse, J., and Salkeld, A. (1980) *Proc. Natl. Acad. Sci. USA.* **77**, 6086-6090

70. McCarrey, J.R., Geyer, C.B., and Yoshioka, H. (2005) *N.Y. Acad. Sci.* **1061**, 226-242

71. McCarrey, J.R., Berg, W.M., Paragioudakis, S.J., Zhang, P.L., Dilworth, D.D., Arnold, B.L., Rossi, J.J. (1992) *Dev. Biol.* **154**, 160-168

72. Ohta, H., Yomogida, K., Tadokoro, Y., Tohda, A., Dohmae, K., and Nishimune, Y. (2001) *Int. J. Androl.* **24**, 15-23

73. Bradley, J., Baltus, A., Skaletsky, H., Royce-Tolland, M., Dewar, K., and Page, D.C. (2004) *Nat. Genet* **36**, 872-876

74. Bailey, J., Evans, J.P., Hardy, M., Herr, J.C., Loveland, K., Matsumoto, A., Trasler, J., Turek, P.J., Vasquez-Levin, M., and Wang, C. Synopsis: 2005 annual meeting of the American Society of Andrology. **26**, 678-688

75. Toder, R., and Graves, J.A.M. (1998) *Mamm. Gen.* **9**, 373-376

76. Nakada, K., Sato, A., Yoshido, K., Morita, T., Tanaka, H., Inoue, S., Yonekawa, H., Hayashi, J. (2006) *Proc. Natl. Acad. Sci. USA.* **103(41)**, 15148-15153

77. Henshaw, S.K. (1998) Unintended pregnancy in the US. *Fam. Plan. Perspect* **30**, 24–29

78. Piccinino, L.J., and Mosher, W.D. (1998) Trends in contraceptive use in the United States: 1982–1995. *Fam. Plan. Perspect* **30**, 4–10

79. Amory, J.K., Page, S.T., and Bremner, W.J. (2006) Drug insight: recent advances in male hormonal contraception. *Nat. Clin. Practice* **2**, 32-41

80. Heinemann, K., Saad, F., Wiesemes, M., White, S., and Heinemann, L. (2005) Attitudes toward male fertility control: results of a multinational survey on four continents. *Hum. Reprod.* **20**, 549–556

81. Martin, C.W., Anderson, R.A., Cheng, L., Ho, P.C., van der Spuy, Z., Smith, K.B., Glasier, A.F., Everington, D., and Baird, D.T. (2000) *Human Reprod.* **15**, 637–645

82. Glasier, A.F., Anakwe, R., Everington, D., Martin, C.W., van der Spuy, Z., Cheng, L., Ho, P.C., and Anderson, R.A. (2000) *Human Reprod* **15**, 646–649

BIOGRAPHICAL SKETCH

Jeffrey V. Brower was born in Hicksville, New York, where he lived for eight years. He and his family then moved to Saint Augustine, Florida, where he attended fourth grade. After staying briefly in Florida, he and his family returned to Long Island, New York, where he would finish his secondary education. Following graduation from high school, he then returned with his family to Florida. Jeffrey received his BS in microbiology and cell science with a minor in chemistry from the University of Florida in 2004. Jeffrey decided to stay at the University of Florida for graduate school, and in 2008, he received his Ph.D in the molecular cell biology concentration of medical sciences in the laboratory of Naohiro Terada, M.D., Ph.D. His work focused on determining the function of a newly discovered member of the adenine nucleotide translocase family of genes, Ant4. This work led him to the identification of an essential function for Ant4, which he found to by germ cell specific, in the process of spermatogenesis. Jeffrey has been accepted to medical school at the University of Florida and will begin in August of 2008. He hopes to continue his research endeavors focusing more on the clinical aspects of medicine while integrating his knowledge of the basic sciences.